Submitted to *INFORMS Journal on Computing*
manuscript (Please, provide the mansucript number!)

Dynamic Compressor Optimization in Natural Gas Pipeline Systems

Terrence W.K. Mak
Data61, Australian National University, and University of Michigan. wmak@umich.edu

Pascal Van Hentenryck
Industrial & Operations Engineering, University of Michigan. pvanhent@umich.edu

Anatoly Zlotnik
Center for Nonlinear Studies, Theoretical Division, Los Alamos National Laboratory. azlotnik@lanl.gov

Russell Bent
A-1: Information & Systems Modeling, Los Alamos National Laboratory. rbent@lanl.gov

The growing dependence of electric power systems on gas-fired generators to balance fluctuating and intermittent production by renewable energy sources has increased the variation and volume of flows withdrawn from natural gas transmission pipelines. Adapting pipeline operations to maintain efficiency and security under these dynamic conditions requires optimization methods that account for substantial intra-day transients and can rapidly compute solutions in reaction to generator re-dispatch. Here, we present a computationally efficient method for minimizing gas compression costs under dynamic conditions where deliveries to customers are described by time-dependent mass flows. The optimization method uses a simplified representation of gas flow physics, provides a choice of discretization schemes in time and space, and exploits a two-stage approach to minimize energy costs and ensure smooth and physically meaningful solutions. The resulting large-scale nonlinear programs are solved using an interior-point method. The optimization scheme is validated by comparing the solutions with an integration of the dynamic equations using an adaptive time-stepping differential equation solver, as well as a different, recently proposed optimal control scheme. The comparison shows that solutions to the discretized problem are feasible for the continuous problem and also practical from an operational standpoint. The results also indicate that our scheme produces at least an order of magnitude reduction in computation time relative to the state-of-the-art and scales to large gas transmission networks with more than 6000 kilometers of total pipeline.

Key words: nonlinear control, optimization, natural gas pipeline systems

Nomenclature

$\mathscr{G} = (\mathscr{J}, \mathscr{P})$	Gas network with a set of junctions $J_i \in \mathscr{J}$ and a set of pipes $P_{ij} \in \mathscr{P}$
$\mathscr{C} \subseteq \mathscr{P}$	Subset of pipes with compressors
p_{ij}	Pressure variable (Pa) for P_{ij}

q_{ij}	Mass flux variable (kg/s) for P_{ij}
p_N, q_N	Pressure and flux dimensionless scaling constants
R_{ij}, c_{ij}	Compressor ratio and compressor location of P_{ij}
d_i	Mass flux (kg/s) injections/consumptions at J_i
s_i	Boundary pressure (Pa) at J_i
S_{ij}	Cost of the compressor at $P_{ij} \in \mathscr{C}$
D_{ij}, A_{ij}, L_{ij}	Pipe diameter (m), cross-section area (m^2), and length (m) of pipe P_{ij}
T	Total time horizon (sec)
γ, η	Isentropic coefficient of gas and compressor efficiency factor
a, λ	Sound speed (ms^{-1}) and gas friction factor
$\overline{p_{ij}}, \underline{p_{ij}}$	Maximum/Minimum pressure limit (Pa)
$\overline{R_{ij}}, \underline{R_{ij}}$	Maximum/Minimum compression limit
x_{ij}, t	Space segment of P_{ij} in $[0..L_{ij}]$ and time point in $[0..T]$

1. Introduction

In recent decades, the increasing penetration of renewable energy sources into electric power grids and the growth in availability of natural gas has driven installation of gas-fired electric power plants to meet most of the demand for new generating capacity and reserves [1, 2, 3]. Gas-fired generators often go online and shut down several times a day, and can rapidly adjust their production, which makes them attractive resources to use for balancing the fluctuation of renewable energy sources such as wind and solar [4, 5, 6].

Historically, withdrawals from natural gas transmission systems came from utilities and industrial consumers whose usage is predictable and exhibits low variation in demand [6]. These withdrawals are traded using day-ahead contracts for fixed deliveries and implicitly assume that injections and withdrawals remain nearly constant [7]. As a result, optimization approaches for natural gas transmission systems have traditionally restricted attention to steady-state models [8, 9].

For example, early studies [10, 11] focused on optimizing steady-state gas flows, for which the state equations are algebraic relations. Recent efforts have scaled and improved optimization techniques for similar problems [12, 13, 14, 15, 16]. In short-term operations, the operating set-points for gas compressor stations can be readily changed, and compressor optimization for steady-state flows has been solved in the form of an optimal gas flow (OGF) [14].

However, the growing use of gas-fired power plants for electricity generation [3, 17] has prompted concerns in both industry sectors [5]. The integration of electric and gas systems may result in gas-fired generator dispatch and commitment schedules that create substantial intra-day fluctuations in high-volume gas flows. The physics underlying these fuctuations cannot be adequately captured by steady-state models [18, 19], raising challenges highlighted in recent studies [20]. To enable natural gas systems to inter-operate with electric power systems on the time-scale of generator dispatch, the OGF must take into account transient flow conditions and new optimization models are required to capture the gas dynamics in pipeline networks [21]. In particular, an automatic control methodology for optimally managing transient intra-day flows in gas transmission systems necessitates stable, accurate, physics-based, and efficient optimization algorithms for computing model-based compressor control protocols.

Gas pipeline flow dynamics over appropriate spatial and temporal scales do not experience waves or shocks, and can be represented by Euler equations for compressible gas flow in one-dimension with significant simplifications [22, 23]. These partial differential equations (PDEs) are highly nonlinear however, and are challenging to simulate, particularly for networks coupling hundreds of equations over different domains [24]. The vast majority of previous studies on gas pipeline transients have focused on physical modeling and simulation of initial value problems (IVPs) [25, 26, 27]. An excellent review of early literature was written by Thorley et al. [28]. However, the traditional approaches to finding solutions to PDEs require fine space-time discretizations that are not tractable for representing dynamic constraints in optimization problems.

The nonlinearity and complexity of gas pipeline network dynamics is also an obstacle to the tractable optimization of these flows under transient conditions. Several studies have proposed optimization schemes for gas networks on the time-scale of daily operations and the issues of computation time and scalability have been noted repeatedly. These optimization methods are focused on producing time-dependent schedules of compressor discharge pressures that satisfy pipeline constraints and meet time-varying loads. These computations are typically very expensive and often too slow for real-time decision-making. This motivates the need for new optimization tools.

Existing approaches for optimization of gas pipelines with dynamics typically fall into one of two categories. Simulation-based methods optimize controllable parameters and rely on repeated executions of high-fidelity simulations to verify that inequality constraints such as pressure limits are satisfied [29, 30]. By solving initial value problems (IVPs) based on highly detailed physical and engineering models to evaluate the dynamic constraints, such methods provide strong guarantees that all constraints are satisfied for feasible solutions. These methods are augmented with adjoint-based gradients [31]. While adjoint methods exploit sparsity and parallelization, higher order derivatives and Jacobians of the active constraints, both of which accelerate convergence and aid robustness, are computationally costly.

Alternatively, discretize-then-optimize approaches are focused on rapid evaluation of constraint Jacobians for the entire optimization period [32]. These approaches start with optimal control formulations that incorporate a cost objective, equality and inequality constraints on state variables, and differential-algebraic approximations of PDE dynamic constraints directly within the optimization problem (instead of relying on simulations). The entire problem is discretized in time using approximations of the functions evaluated at time- and space- collocation points, using local difference schemes [33] or spectral approximation [34]. The resulting model is a nonlinear program (NLP) with purely algebraic objective and constraint functions. Although this type of formulation may be large-scale, it can be solved by taking advantage of special structure or by recently developed general optimization tools for problems with sparse constraints [35].

Recently developed approaches to reduced order representation of PDE dynamics on graphs [36], and their extension to control system modeling [34, 35], have enabled tractable representations of gas pipeline system dynamics. Such models are used to express constraints in dynamic optimization problems as well as to perform simulations of IVPs. In the former case, the constraints over the entire optimization time interval are represented using a coarse discretization. In the latter case, fine-grained time stepping is used to compute the solution forward over the simulation time interval. Here, we show that using a "discretize-then-optimize" approach on a coarser grid than those used in simulation-based approaches results in solutions with low error rates and significantly improved computation times.

This paper examines the Dynamic Optimal Gas Flow (DOGF) problem, which generalizes the OGF to capture the dynamics of a gas pipeline network subject to time-dependent intra-day consumptions. The objective of the DOGF is to minimize the cost of gas compression subject to system pressure constraints and time-dependent flow withdrawals. Our main contribution is a computationally efficient optimization scheme for the DOGF, that is validated with an accurate simulation method for gas pipeline networks with dynamic flows and compressor operations. The DOGF is formulated for optimizing intra-day flow schedules, and therefore, does not consider valves as controllable variables. Major topological changes for re-routing flows by changing valve positions are typically made on a weekly or monthly basis. By fixing the system topology, we formulate the DOGF as a continuous-time, continuous-state optimal control problem that is discretized as a nonlinear program with continuous variables only. Generalizing the problem to include valves significantly increases model complexity by adding a large number of binary variables. This addition is outside of the scope of the present work but is an important topic for further research in energy systems in general.

The key aspects of our optimization scheme are summarized as follows. The hydrodynamic relations that describe gas flows are discretized in time and space using first-order approximations [34]. Several relaxations of the nonlinear constraints are proposed: The spatial discretization is performed by either the trapezoidal rule or a lumped element approximation, while the temporal discretization employs either a trapezoidal rule or a pseudospectral approximation. While trapezoidal, lumped element, and similar space-discretization schemes have been used in simulation studies [28, 36], pseudospectral schemes are often used for time discretization in computational optimal control [37]. For various combinations of discretizations in time and space, we investigate the trade-offs between computational efficiency of the optimization and feasibility of the physical model, as verified by a fine-grained simulation. While a significant theory exists on convergence of computational optimal control methods based on pseudospectral approximation [38, 39], such schemes are dense and global on the time interval of interest. Simpler, local differentiation rules support sparse computations that yield faster, more accurate solutions. We find that, for the DOGF problem, the combination of lumped elements in space and trapezoidal rule in time yields the most advantageous discretization in this respect.

In general, time and space discretizations for PDEs cannot be chosen independently. In this study, we focus on practical algorithmic aspects of dynamic optimization of pipeline transients, rather than the theoretical justifications of particular discretization schemes for parabolic PDE systems. We support the resulting optimization approach by empirically comparing the solution of the dynamic constraints (pressures and flows) to solutions using a validated high-fidelity simulation of the same constraints. The time and space discretization procedures are applied sequentially in the schemes proposed here. This approach is inspired by the simulation methodology for solving initial value problems [34, 36], in which the uniform lumped element space discretization yields a differential algebraic equation (DAE) system on a fixed space grid. Starting from initial conditions, the equations are integrated forward in time using adaptive stepping, thus falling into the class of method of lines (MOL) approaches [40]. Therefore, we apply time-discretization to the dynamic constraints after they have been discretized in space, and examine the quality of solutions empirically based on several case studies.

Moreover, to compensate for potential inaccuracies and model operational constraints on compressors, the paper proposes a two-stage optimization approach. In the first stage, the scheme optimizes the compression cost (the original objective). In order to obtain a solution that appropriately represents smooth fluid flow physics and operational considerations, the second stage minimizes the time derivative of the compressor boost ratios while ensuring that the overall compression costs remain close to the value found in the first stage. The resulting large-scale, nonlinear optimization problems (with up to 130,000 decision variables) are solved using the IPOPT 3.12.2, ASL routine (version 2015) nonlinear optimization system [41].

The solutions produced by our optimization scheme are compared to a validated dynamic simulation method for gas pipeline networks with transient compression [42, 43], which is parametrized by the compressor ratios from our optimized solutions. The validation process indicates that our optimization scheme produces solutions with no pressure constraint violations and with physically meaningful mass flow and pressure trajectories that match well the corresponding simulations. Moreover, the compressor ratios from our four discretization variants exhibit negligible differences and eventually converge to the same solution. The main benefit of our optimization scheme, however, is its computational efficiency. It provides a highly accurate solution to a previously investigated 24-pipe gas network case study in less than 30 seconds, and demonstrates scalability to pipeline networks with 25, 40, and 135 nodes, 24, 45, and 170 pipes, and with total pipeline lengths of 477, 1118, and 6964 kilometers respectively.

Preliminary results of our work were published in the proceedings of the 2016 American Control Conference [35], where the trapezoidal rule was used for discretization in both time and space. This paper extends our previous work by presenting and comparing four discretization schemes in detail, as well as by developing initial formulations for maximizing system throughput or operator revenue in the presence of highly variable loads.

The rest of the paper is organized as follows. Section 2 contains a summary of physical modeling of gas pipeline networks, and formulates the DOGF. Section 3 describes the discretization schemes that we examine. Section 4 motivates and presents our two-stage optimization approach to enforce smooth, physically accurate solutions. Section 5 describes computational and validation results for three case studies on systems of increasing scale and complexity. Section 6 concludes with a discussion and summary of possible future directions.

2. Compressor Optimization in Gas Pipelines

A gas pipeline network can be represented as a directed graph $\mathcal{G} = (\mathcal{J}, \mathcal{P})$, where edges $\{i, j\} \in \mathcal{P}$ represent pipes P_{ij} connecting nodes $i, j \in \mathcal{J}$ representing junctions J_i and J_j. The length of pipe P_{ij} is denoted by L_{ij}, its diameter by D_{ij}, and its cross-sectional area by A_{ij}. The dynamic state on the pipe P_{ij} at a location $x_{ij} \in [0, L_{ij}]$ and time $t \in [0, T]$ is given by pressure $p_{ij}(t, x)$ and mass flow $q_{ij}(t, x)$ functions.

We are interested in the subsonic and isothermal regime where transients are sufficiently slow so as not to excite shocks or waves, i.e., where the flow velocity through a pipe is less than the speed of sound a in the gas, and temperature is assumed to be constant. Major changes in gas temperature generally occur because of gas compression. Since nearly all gas pipelines are buried under ground (with a few exceptions, e.g., river crossings), the gas temperature returns to ground temperature one or two kilometers downstream of compression [44]. Because the variation in absolute ground temperature outside the neighborhood of compressor stations is on the order of a few percent, and because modern compressor stations are equipped with gas coolers, we assume that there are no large temperature differences in the network.

The flow dynamics on a single pipe P_{ij} can be adequately described in this regime [23] by:

$$\frac{\partial p_{ij}}{\partial t} + \frac{a^2}{A_{ij}} \frac{\partial q_{ij}}{\partial x} = 0 \tag{1}$$

$$\frac{1}{A_{ij}} p_{ij} \frac{\partial q_{ij}}{\partial t} + p_{ij} \frac{\partial p_{ij}}{\partial x} = -\frac{\lambda a^2}{2 D_{ij} A_{ij}^2} q_{ij} |q_{ij}|, \tag{2}$$

and further reduced [23], by approximating $\frac{\partial q_{ij}}{\partial t} \approx 0$, to

$$\frac{\partial p_{ij}}{\partial t} + \frac{a^2}{A_{ij}} \frac{\partial q_{ij}}{\partial x} = 0 \tag{3}$$

$$2 p_{ij} \frac{\partial p_{ij}}{\partial x} + \frac{\lambda a^2}{D_{ij} A_{ij}^2} q_{ij} |q_{ij}| = 0 \tag{4}$$

We used the modeling assumptions outlined in [22], which is validated and widely used in other studies on modeling of gas pipeline networks for optimization with dynamics [6, 23, 35]. In addition to omitting higher-order inertial terms and gravity effects from the flow equations, we assume that gas composition and temperature are uniform throughout the network, and a nominal value for gas compressibility is chosen. This results in a constant, system-wide value for the speed of sound in the gas. Thus, the speed of sound a is assumed to be uniform and constant throughout the system. Our focus here is on the development and validation of an optimization methodology for dynamics, rather than on detailed physical modeling. We are focused on capturing the key physical phenomena of large-scale gas pipeline flows. The second term in (4) approximates friction effects, which constitute the major phenomenon that dissipates momentum of the gas flow [22]. We leave for future work the generalizations of our results to cases where temperature and gas composition are inhomogeneous and an equation of state determines gas compressibility.

The gas dynamics on a pipeline segment are represented using (3)-(4) and possess a unique solution when any two of the boundary conditions $p_{ij}(t,0)$, $q_{ij}(t,0)$, $p_{ij}(t,L_{ij})$, or $q_{ij}(t,L_{ij})$ are specified. For both computational and notational purposes, we apply a transformation to dimensionless variables [23] given by

$$\tilde{p}_{ij} = \frac{p_{ij}}{p_N}, \qquad \tilde{q}_{ij} = \frac{q_{ij}}{q_N}, \qquad \tilde{x}_{ij} = x\frac{\lambda a^2 q_N^2}{D_{ij}A_{ij}^2 p_N^2}, \qquad \tilde{t}_{ij} = t\frac{\lambda a^4 q_N^3}{D_{ij}A_{ij}^3 p_N^3}, \tag{5}$$

where p_N and q_N are scaling constants. This results in the dimensionless equations

$$\frac{\partial \tilde{p}_{ij}}{\partial \tilde{t}_{ij}} + \frac{\partial \tilde{q}_{ij}}{\partial \tilde{x}_{ij}} = 0, \tag{6}$$

$$2\tilde{p}_{ij}\frac{\partial \tilde{p}_{ij}}{\partial \tilde{x}_{ij}} + \tilde{q}_{ij}|\tilde{q}_{ij}| = 0, \tag{7}$$

Note that the space and time variables x_{ij} and t_{ij} are now pipe-dependent. Design limits and regulations for pipeline systems require pressure to remain within specified bounds given by

$$\underline{\tilde{p}}_{ij} \le \tilde{p}_{ij}(\tilde{t}_{ij},\tilde{x}_{ij}) \le \overline{\tilde{p}}_{ij}. \tag{8}$$

The momentum dissipation due to the friction term in (4) causes the gas pressure to decrease, hence it must be augmented by compressors to maintain the minimum required pressure. We define $\mathscr{C} \subseteq \mathscr{P}$ as the subset of pipes that have compressors. The action of compressors is modeled as a conservation of flow and an increase in pressure at a point $c_{ij} \in [0,L_{ij}]$ by a multiplicative ratio $R_{ij}(\tilde{t}_{ij}) \ge 1$ that may depend on time.

Specifically,

$$\lim_{\tilde{x}_{ij}\searrow c_{ij}} \tilde{p}_{ij}(\tilde{t}_{ij},\tilde{x}_{ij}) = R_{ij}(\tilde{t}_{ij}) \lim_{\tilde{x}_{ij}\nearrow c_{ij}} \tilde{p}_{ij}(\tilde{t}_{ij},\tilde{x}_{ij}), \tag{9}$$

$$\lim_{\tilde{x}_{ij}\searrow c_{ij}} \tilde{q}_{ij}(\tilde{t}_{ij},\tilde{x}_{ij}) = \lim_{\tilde{x}_{ij}\nearrow c_{ij}} \tilde{q}_{ij}(\tilde{t}_{ij},\tilde{x}_{ij}). \tag{10}$$

The cost of compression S_{ij} is proportional to the required power [45], and is approximated by

$$S_{ij}(\tilde{t}_{ij}) = \eta^{-1}|\tilde{q}_{ij}(\tilde{t}_{ij},c_{ij})|(\max\{R_{ij}(\tilde{t}_{ij}),1\}^{2K}-1) \tag{11}$$

with $0 < K = (\gamma - 1)/\gamma < 1$, where γ is the heat capacity ratio and η is a compressor efficiency factor. In this study we do not consider pressure regulation (decompression), so the compressor ratio for a given station must remain bounded within a feasible operating region

$$\max\{\underline{R}_{ij}, 1\} \leq R_{ij} \leq \overline{R}_{ij}. \tag{12}$$

A compression ratio with a value greater than 1, i.e., $R_{ij}(\tilde{t}_{ij}) \geq 1$, corresponds to a compressor applying power in its defined working direction. A value of $R_{ij}(\tilde{t}_{ij}) = 1$ denotes a compressor that is bypassed by the flow, in either the working or the reverse direction. For modeling flows in large-scale systems, we use theoretical compressors that represent entire compressor stations as single objects. For transmission pipelines, flow to all machinery in the station is accepted and discharged through common headers. The detailed control mechanisms of individual compressors are abstracted, and individual compressors are coordinated by the control system of the station to maintain operating setpoints corresponding to the common headers. This abstract representation of actuators that boost pressure can also be used to model pressure regulators that decrease the pressure where needed. However, large-scale transmission pipelines typically include few such elements, because regulation is often performed to lower pressure at city gates or large customers after custody is transferred from the pipeline.

This study does not model regulators and makes certain assumptions on the structure of the system and the pressure bounds. We assume that the pipeline system was built in order to admit feasible solutions in its usual operations. Specifically, since pressure cannot be actively decreased in our model (in accordance with the typical construction of transmission pipelines), we assume that the maximum pressure bound throughout the network is uniform. While this may appear to be a strong assumption, it is reasonable in practice as: 1) the intra-day operation of high-pressure, large-scale transmission systems is separated from operation of lower pressure distribution systems, and 2) transmission systems rarely experience changes in large-scale flow directions. This assumption guarantees that R_{ij} must be assigned to 1 (set to bypass mode) in the optimal solution if gas is delivered in the reverse direction (from j to i) on a pipe P_{ij} with compressor C_{ij}. Indeed, assume that R_{ij} is larger than 1 (i.e., set to regulator mode in the reverse flow direction) in an optimal solution. Because the maximum pressure bound is uniform across the network, it is possible to remove the decompression and obtain a feasible solution with a lower cost based on our objective function, contradicting the optimality assumption. This means that $R_{ij} = 1$ when the flow is reversed on pipe P_{ij}. The investigation of appropriate models and optimal control problems for systems with more complex structure, such as multi-pressure systems that require intra-day control of regulators, is a topic for future research.

In addition to the dynamic equations (6)-(7) and continuity conditions for compressors (9)-(10) that characterize the system behavior on each pipe $P_{ij} \in \mathscr{P}$, we specify balance conditions for each junction $J_i \in \mathscr{J}$. We first define variables for the unique nodal pressure $p_i(t)$ at each junction, as well as mass injections $f_i(t)$ from outside the system (negative for withdrawals/consumption).

Each junction $J_j \in \mathscr{J}$ then has a flow balance condition

$$\sum_{J_k \in \mathscr{J}: P_{jk} \in \mathscr{P}} \tilde{q}_{jk}(\tilde{t}_{ij}, 0) - \sum_{J_i \in \mathscr{J}: P_{ij} \in \mathscr{P}} \tilde{q}_{ij}(\tilde{t}_{ij}, L_{ij}) = f_j(t), \tag{13}$$

as well as a pressure continuity condition

$$\tilde{p}_{ij}(\tilde{t}_{ij}, L) = p_j(t) = p_{jk}(\tilde{t}_{ij}, 0), \qquad \forall J_i, J_k \in \mathscr{J} \text{ s.t. } P_{ij}, P_{jk} \in \mathscr{P} \tag{14}$$

where $\tilde{t}_{ij}$ is the pipe-dependent dimensionless time transformed from the time t in nominal unit.

A subset of the junctions $\mathscr{S} \subset \mathscr{J}$ may be treated as "slack" nodes, which reasonably represent large sources in a transmission system, such as significant storages or interconnections. For these junctions, the mass inflow $f_i(t)$ is a free variable and the nodal pressure is defined at a supply pressure boundary parameter $s_i(t)$ (in dimensionless unit). For the remaining junctions, which reasonably represent consumers or small suppliers, the nodal pressure $p_i(t)$ is free and the mass inflow is initialized with an injection/withdrawal boundary parameter $d_i(t)$ (in dimensionless unit). These boundary conditions are given by

$$p_i(t) = s_i(t), \qquad f_i(t) = d_i(t). \tag{15}$$

Here, we express injections into and withdrawals from the pipeline network in terms of mass flow. While the contracts and daily nominations for natural gas are given in units of energy, e.g., kWh or mmBtu, the assumption of uniform system-wide composition allows the use of mass flow units. In practice, the mass flow nominated depends on the calorific value, which is normally assumed to be known at the sources. Our focus is on large-scale transmission pipelines that receive gas from processing plants, which supply gas with composition with less than 2% variability. Preliminary validation on real data of transmission pipeline modeling using density and mass flow variables only has recently shown the approach to be acceptable in an industrial setting [46].

The optimization problem that we solve involves a gas pipeline network for which the conditions at each junction are parameterized by an injection/withdrawal $d_i(t)$ or supply pressure $s_i(t)$. The design goal is for the system to deliver all of the required flows $d_i(t)$ while maintaining feasible system pressure given the physics-based dynamic constraints, and minimizing the cost of compression over a time interval $[0,T]$. Let $\tilde{T}_{ij} = T\frac{\lambda a^4 q_N^3}{D_{ij}A_{ij}^3 p_N^3}$ to be the dimensionless time horizon of P_{ij}. This cost objective is given by

$$C = \sum_{P_{ij}\in\mathscr{C}} \int_0^{\tilde{T}_{ij}} S_{ij}(\tilde{t}_{ij})\mathrm{d}\tilde{t}_{ij} \tag{16}$$

In this study, we consider time-periodic boundary conditions on the system state and controls, i.e.,

$$\tilde{p}_{ij}(0,\tilde{x}_{ij}) = \tilde{p}_{ij}(\tilde{T}_{ij},\tilde{x}_{ij}), \tilde{q}_{ij}(0,\tilde{x}_{ij}) = \tilde{q}_{ij}(\tilde{T}_{ij},\tilde{x}_{ij}), \forall P_{ij} \in \mathscr{P} \tag{17}$$

$$R_{ij}(0) = R_{ij}(\tilde{T}_{ij}), \quad \forall P_{ij} \in \mathscr{C} \tag{18}$$

and therefore feasible parameter functions also must satisfy $d_i(0) = d_i(T)$ and $s_i(0) = s_i(T)$. The complete formulation is

$$\begin{aligned}
&\min\ C \text{ in } (16) \\
&s.t.\ \ \text{pipe dynamics: } (6),(7) \\
&\qquad\ \text{compressor continuity: } (9),(10) \\
&\qquad\ \text{junction conditions: } (13),(14) \\
&\qquad\ \text{density \& compression constraints: } (8),(12) \\
&\qquad\ \text{periodicity constraints: } (17),(18) \\
&\qquad\ \text{boundary parameters: } (15) \\
&\qquad\ \text{compressor power: } (11)
\end{aligned} \tag{19}$$

In the next section, we describe a spatial and temporal discretization scheme and relaxation conditions that facilitate efficient solution of this PDE-constrained optimization problem using standard nonlinear programming tools.

3. Discretization to a Nonlinear Program

We evaluate several discretization schemes to balance the high nonlinearity in the spatiotemporal dynamics (6)-(7) among a collection of auxiliary variables in which the constraints in Problem (19) possess a sparse representation. In all of our schemes, we will have the following common notions. For each pipe P_{ij}, we have: 1) a set of $M+1$ time points $\tilde{t}_m^{ij}$, and 2) a set of $N_{ij}+1$

space points $\tilde{x}_n^{ij}$. Normalization and rescaling is performed after choosing the collocation points identically throughout the network in order to maintain consistency of the time discretization. We use a uniform grid for the trapezoidal scheme for simplicity. For pseudospectral methods, the collocation points are chosen according to the polynomial approximation scheme.

3.1. Trapezoidal Quadrature Rule Approximation

For trapezoidal discretization, we discretize $\tilde{t}_m^{ij}$ and $\tilde{x}_n^{ij}$ uniformly:

$$\tilde{t}_m^{ij} = m\Delta_{ij}^t, \quad m = 0,1,\ldots,M, \tag{20}$$

$$\tilde{x}_n^{ij} = n\Delta_{ij}^x, \quad m = 0,1,\ldots,N_{ij}, \tag{21}$$

$$\Delta_{ij}^t = \frac{\tilde{T}_{ij}}{M}, \quad \Delta_{ij}^x = \frac{\tilde{L}_{ij}}{N_{ij}}. \tag{22}$$

Δ_{ij}^t and Δ_{ij}^x are (dimensionless) time and space discretization steps, and $\tilde{T}_{ij}$ is the dimensionless time horizon for pipe P_{ij} obtained from T according to (5). We omit the subscripts $\{ij\}$ on N_{ij} when they are clear from the context. For each of the $(M+1)\times(N_{ij}+1)$ discrete points in the time-space grid $\{(\tilde{t}_m^{ij},\tilde{x}_n^{ij}) : 0 \le m \le M, 0 \le n \le N_{ij}\}$ within the (dimensionless) domain $[0,\tilde{T}_{ij}]\times[0,\tilde{L}_{ij}]$ for the flow dynamics on a pipe P_{ij}, we define

$$\tilde{p}_{ij}^{mn} \triangleq \tilde{p}_{ij}(\tilde{t}_m^{ij},\tilde{x}_n^{ij}), \quad \tilde{q}_{ij}^{mn} \triangleq \tilde{q}_{ij}(\tilde{t}_m^{ij},\tilde{x}_n^{ij}) \tag{23}$$

to be the pressure and mass flow variables at time $\tilde{t}_m^{ij}$ and location $\tilde{x}_n^{ij}$. In this discretization, we define temporal and spatial derivative variables at time $\tilde{t}_m^{ij}$ and location $\tilde{x}_n^{ij}$ by

$$\tilde{pt}_{ij}^{mn} \triangleq \frac{\partial \tilde{p}_{ij}}{\partial \tilde{t}_{ij}}(\tilde{t}_m^{ij},\tilde{x}_n^{ij}), \quad \tilde{px}_{ij}^{mn} \triangleq \frac{\partial \tilde{p}_{ij}}{\partial \tilde{x}_{ij}}(\tilde{t}_m^{ij},\tilde{x}_n^{ij}), \tag{24}$$

$$\tilde{qx}_{ij}^{mn} \triangleq \frac{\partial \tilde{q}_{ij}}{\partial \tilde{x}_{ij}}(\tilde{t}_m^{ij},\tilde{x}_n^{ij}). \tag{25}$$

A constraint that relates the discretized variables (23) to their derivatives (24)-(25) is created by approximating the integral over a time or space step by the trapezoid rule. This yields

$$\forall P_{ij} \in \mathscr{P} - \mathscr{C}, 0 \le m \le M-1, 0 \le n \le N : \quad \tilde{p}_{ij}^{m+1,n} - \tilde{p}_{ij}^{mn} \approx \frac{\Delta_{ij}^t}{2}(\tilde{pt}_{ij}^{m+1,n} + \tilde{pt}_{ij}^{mn}) \tag{26}$$

$$\forall P_{ij} \in \mathscr{P} - \mathscr{C}, 0 \le m \le M, 0 \le n \le N-1 :$$

$$\tilde{p}_{ij}^{m,n+1} - \tilde{p}_{ij}^{mn} \approx \frac{\Delta_{ij}^x}{2}(\tilde{px}_{ij}^{m,n+1} + \tilde{px}_{ij}^{mn}), \quad \tilde{q}_{ij}^{m,n+1} - \tilde{q}_{ij}^{mn} \approx \frac{\Delta_{ij}^x}{2}(\tilde{qx}_{ij}^{m,n+1} + \tilde{qx}_{ij}^{mn}) \tag{27}$$

3.2. Non-dimensional Dynamic Equation with Compressors

The non-dimensional dynamic equations (6)-(7) are then discretized in the above variables by

$$\forall P_{ij} \in \mathscr{P} - \mathscr{C}, 0 \leq m \leq M, 0 \leq n \leq N: \quad \tilde{pt}_{ij}^{mn} + \tilde{qx}_{ij}^{mn} = 0, \quad 2\tilde{p}_{ij}^{mn}\tilde{px}_{ij}^{mn} + \tilde{q}_{ij}^{mn}|\tilde{q}_{ij}^{mn}| = 0 \tag{28}$$

For each pipe with compressors $P_{ij} \in \mathscr{C}$, we define the discrete compression variables R_{ij}^m for $m = 0, 1, \ldots, M$, and assume that the compressor is located at $c_{ij} = x_k$ for some $0 \leq k \leq N$, where the dependence of k on the pipe P_{ij} in question is clear from the context. The pipe is then divided into two pipes P_{iju} and P_{ijl}, with non-dimensional lengths L_{iju} and L_{ijl}, and for which we define the discretized variables

$$\tilde{p}_{iju}^{mn} \stackrel{\Delta}{=} \tilde{p}_{ij}(\tilde{t}_m^{ij}, \tilde{x}_n^{ij}), \quad \tilde{q}_{iju}^{mn} \stackrel{\Delta}{=} \tilde{q}_{ij}(\tilde{t}_m^{ij}, \tilde{x}_n^{ij}), \quad 0 \leq n \leq k \tag{29}$$

$$\tilde{p}_{ijl}^{mn} \stackrel{\Delta}{=} \tilde{p}_{ij}(\tilde{t}_m^{ij}, \tilde{x}_n^{ij}), \quad \tilde{q}_{ijl}^{mn} \stackrel{\Delta}{=} \tilde{q}_{ij}(\tilde{t}_m^{ij}, \tilde{x}_n^{ij}), \quad k \leq n \leq N \tag{30}$$

and corresponding spatial derivative variables $\tilde{pt}_{iju}^{mn}$, $\tilde{px}_{iju}^{mn}$, and $\tilde{qx}_{iju}^{mn}$ for $0 \leq n \leq k$ and $\tilde{pt}_{ijl}^{mn}$, $\tilde{px}_{ijl}^{mn}$, and $\tilde{qx}_{ijl}^{mn}$ for $k \leq n \leq N$. These state and derivative variables satisfy

$$\tilde{p}_{iju}^{m+1,n} - \tilde{p}_{iju}^{mn} \approx \frac{\Delta_{ij}^t}{2}(\tilde{pt}_{iju}^{m+1,n} + \tilde{pt}_{iju}^{mn}), \quad 0 \leq n \leq k, \tag{31}$$

$$\tilde{p}_{ijl}^{m+1,n} - \tilde{p}_{ijl}^{mn} \approx \frac{\Delta_{ij}^t}{2}(\tilde{pt}_{ijl}^{m+1,n} + \tilde{pt}_{ijl}^{mn}), \quad k \leq n \leq N \tag{32}$$

for $P_{ij} \in \mathscr{C}$ and $0 \leq m \leq M-1$, and

$$\tilde{p}_{iju}^{m,n+1} - \tilde{p}_{iju}^{mn} \approx \frac{\Delta_{ij}^x}{2}(\tilde{px}_{iju}^{m,n+1} + \tilde{px}_{iju}^{mn}), \quad 0 \leq n < k, \tag{33}$$

$$\tilde{p}_{ijl}^{m,n+1} - \tilde{p}_{ijl}^{mn} \approx \frac{\Delta_{ij}^x}{2}(\tilde{px}_{ijl}^{m,n+1} + \tilde{px}_{ijl}^{mn}), \quad k \leq n \leq N, \tag{34}$$

$$\tilde{q}_{iju}^{m,n+1} - \tilde{q}_{iju}^{mn} \approx \frac{\Delta_{ij}^x}{2}(\tilde{qx}_{iju}^{m,n+1} + \tilde{qx}_{iju}^{mn}), \quad 0 \leq n < k, \tag{35}$$

$$\tilde{q}_{ijl}^{m,n+1} - \tilde{q}_{ijl}^{mn} \approx \frac{\Delta_{ij}^x}{2}(\tilde{qx}_{ijl}^{m,n+1} + \tilde{qx}_{ijl}^{mn}), \quad k \leq n \leq N \tag{36}$$

for $P_{ij} \in \mathscr{C}$ and $0 \leq m \leq M$. In addition, we require continuity constraints at the compressor location to connect pipes P_{iju} and P_{ijl} for all $P_{ij} \in \mathscr{C}$ and $0 \leq m \leq M$, which take the form

$$R_{ij}^m = \frac{\tilde{p}_{ijl}^{mk}}{\tilde{p}_{iju}^{mk}}, \quad \tilde{q}_{ijl}^{mk} = \tilde{q}_{iju}^{mk}. \tag{37}$$

The equations (6)-(7) on either side of the compressor are discretized for $P_{ij} \in \mathscr{C}$ by

$$\tilde{p}t^{mn}_{iju} + \tilde{q}x^{mn}_{iju} = 0, \quad 0 \le n \le k, \tag{38}$$

$$2\tilde{p}^{mn}_{iju}\tilde{p}x^{mn}_{iju} + \tilde{q}^{mn}_{iju}|\tilde{q}^{mn}_{iju}| = 0, \quad 0 \le n \le k, \tag{39}$$

$$\tilde{p}t^{mn}_{ijl} + \tilde{q}x^{mn}_{ijl} = 0, \quad k \le n \le N \tag{40}$$

$$2\tilde{p}^{mn}_{ijl}\tilde{p}x^{mn}_{ijl} + \tilde{q}^{mn}_{ijl}|\tilde{q}^{mn}_{ijl}| = 0, \quad k \le n \le N \tag{41}$$

for all $P_{ij} \in \mathscr{C}$ and $0 \le m \le M$. The equations (26)-(28) and (31)-(41) discretize the dynamic equations (6)-(7) and continuity conditions for compressors (9)-(10).

3.3. Pseudospectral Approximation

Another approach to time discretization is a pseudospectral approximation, which is a global approximation scheme that is endowed with the desirable properties of spectral accuracy [38]. Here, we use the Legendre-Gauss-Lobatto (LGL) pseudospectral collocation scheme for time discretization [47, 48, 49]. Suppose we want to discretize a function into $M+1$ time points $(\tau_0, \ldots, \tau_M)$. The scheme employs a Legendre polynomial of order M ($L_M(\tau)$) as the interpolant, and the appropriate time collocation points for the discretization are given as the zeros of the derivative of L_M (i.e., the zeros of $\frac{\partial L_M(\tau)}{\partial \tau}$). These points lie within the interval $[-1,1]$, and rescaling (via affine transformation) is required to rescale the time points $\tilde{t}^{ij}_m \in [0, \tilde{T}_{ij}]$ to dimensionless ones of the form $\tau_m \in [-1,1]$. This yields

$$\tau_m = \frac{2\tilde{t}^{ij}_m - \tilde{T}_{ij}}{\tilde{T}_{ij}}, \tag{42}$$

and also induces a re-scaled function f^T on $\tau_m \in [-1,1]$, of form

$$f^T(\tau_m) = f(\tilde{t}^{ij}_m) \text{ where } \tilde{t}^{ij}_m = \frac{\tilde{T}_{ij}(\tau_m + 1)}{2}. \tag{43}$$

The scheme is based on the M^{th} degree interpolating polynomial $f^M(\tau)$, constructed as follows:

$$f^M(\tau) = \sum_{m=0}^{M} f^T(\tau_m)\phi_m(\tau), \text{ where } \phi_m(\tau) = \frac{1}{M(M+1)L_M(\tau_m)} \frac{(\tau^2 - 1)\frac{\partial L_M(\tau)}{\partial \tau}}{\tau - \tau_m}. \tag{44}$$

Because ϕ_m is constructed such that $\phi_m(\tau_j)$ will be 1 if $m = j$ and 0 otherwise, f^M will be equal to f^T on all discretized re-scaled points $(\tau_0, \ldots, \tau_M)$. By restricting our attention to f^M and only at the discretized points, we have the following approximation for differentiation:

$$\frac{\partial f(\tilde{t}^{ij}_m)}{\partial \tilde{t}_{ij}} = \frac{\partial f^T(\tau_m)}{\partial \tau}\frac{\partial \tau}{\partial \tilde{t}_{ij}} \approx \frac{2}{\tilde{T}_{ij}}\frac{\partial f^M(\tau_m)}{\partial \tau} = \sum_{j=0}^{M} D_{mj} f^T(\tau_j) = \sum_{j=0}^{M} D_{mj} f(\tilde{t}^{ij}_j), \quad \forall 0 \le m \le M \tag{45}$$

where D_{mj} is the time differentiation coefficient on the j^{th} Legendre polynomial at time τ_j:

$$D_{mj} = \frac{2}{\tilde{T}_{ij}} \begin{cases} \frac{L_M(\tau_m)}{L_M(\tau_j)} \frac{1}{\tau_m - \tau_j}, & m \neq j \\ -\frac{M(M+1)}{4}, & m = j = 0 \\ \frac{M(M+1)}{4}, & m = j = M \\ 0, & \text{otherwise} \end{cases} \tag{46}$$

We also obtain an expression for integration in $\tilde{t}_{ij}$ from t_a to t_b given by

$$\begin{aligned} \int_{t_a}^{t_b} f(\tilde{t}_{ij}) d\tilde{t}_{ij} = \int_{\tau_a}^{\tau_b} f^T(\tau) \frac{\partial \tilde{t}_{ij}}{\partial \tau} d\tau \approx \frac{\tilde{T}_{ij}}{2} \int_{\tau_a}^{\tau_b} f^M(\tau) d\tau \\ = \frac{\tilde{T}_{ij}(\tau_b - \tau_a)}{2} \sum_{j=0}^{M} [f^T(\tau_j) w_j] = (t_b - t_a) \sum_{j=0}^{M} [f(\tilde{t}_j^{ij}) w_j] \end{aligned} \tag{47}$$

where w_j is the weighting coefficient with respect to the Lagrange polynomial ϕ_j:

$$w_j = \frac{1}{M(M+1)} \frac{1}{(L_M(\tau_j))^2} \tag{48}$$

To change from trapezoidal time discretization to LGL pseudospectral discretization, we replace (26), (31), and (32) by

$$\tilde{pt}_{ij}^{mn} \approx \sum_{g=0}^{M} D_{mg} \tilde{p}_{ij}^{gn} \tag{49}$$

for all $P_{ij} \in \mathscr{P} - \mathscr{C}$, $0 \leq m \leq M$, and $0 \leq n \leq N$, and

$$\tilde{pt}_{iju}^{mn} \approx \sum_{g=0}^{M} D_{mg} \tilde{p}_{iju}^{gn}, \quad 0 \leq n \leq k, \tag{50}$$

$$\tilde{pt}_{ijl}^{mn} \approx \sum_{g=0}^{M} D_{mg} \tilde{p}_{ijl}^{gn}, \quad k \leq n \leq N \tag{51}$$

for $P_{ij} \in \mathscr{C}$ and $0 \leq m \leq M$, where $\tilde{T}_{ij}$ is the pipe-dependent dimensionless time horizon, and k is the compressor location of pipe P_{ij}.

3.4. Lumped Element Approximation

So far, we have approximated equations (6)-(7) by spatial discretization for both the pressure and flux variables and only a time discretization for the pressure variables. One way to further decrease the computational complexity is to simplify the space discretization by using a lumped element approximation, where spatial derivative variables are no longer required. Instead of approximating spatial derivatives by (27) and (33)-(36), a lumped-element approximation is applied to the non-dimensional dynamic equations (6)-(7) by integrating along each pipe segment in space, either explicitly or by the trapezoid quadrature rule. This yields the relations:

$$\int_{\tilde{x}_n^{ij}}^{\tilde{x}_{n+1}^{ij}} \frac{\partial \tilde{p}_{ij}}{\partial \tilde{t}_{ij}} \mathrm{d}\tilde{x}_{ij} \approx \frac{\Delta_{ij}^x}{2}(\tilde{pt}_{ij}^{mn} + \tilde{pt}_{ij}^{m,n+1}), \tag{52}$$

$$\int_{\tilde{x}_n^{ij}}^{\tilde{x}_{n+1}^{ij}} \frac{\partial \tilde{q}_{ij}}{\partial \tilde{x}_{ij}} \mathrm{d}\tilde{x}_{ij} = \tilde{q}_{ij}^{m,n+1} - \tilde{q}_{ij}^{mn}, \tag{53}$$

$$\int_{\tilde{x}_n^{ij}}^{\tilde{x}_{n+1}^{ij}} 2\tilde{p}_{ij} \frac{\partial \tilde{p}_{ij}}{\partial \tilde{x}_{ij}} \mathrm{d}\tilde{x}_{ij} = \int_{\tilde{x}_n^{ij}}^{\tilde{x}_{n+1}^{ij}} \frac{\partial (\tilde{p}_{ij})^2}{\partial \tilde{x}_{ij}} \mathrm{d}\tilde{x}_{ij} = (\tilde{p}_{ij}^{m,n+1})^2 - (\tilde{p}_{ij}^{mn})^2, \tag{54}$$

$$\int_{\tilde{x}_n^{ij}}^{\tilde{x}_{n+1}^{ij}} \tilde{q}_{ij}|\tilde{q}_{ij}| \mathrm{d}\tilde{x}_{ij} \approx \frac{\Delta_{ij}^x}{2}(\tilde{q}_{ij}^{mn}|\tilde{q}_{ij}^{mn}| + \tilde{q}_{ij}^{m,n+1}|\tilde{q}_{ij}^{m,n+1}|) \tag{55}$$

Substituting back into (6)-(7) yields

$$\frac{\Delta_{ij}^x}{2}(\tilde{pt}_{ij}^{mn} + \tilde{pt}_{ij}^{m,n+1}) + \tilde{q}_{ij}^{m,n+1} - \tilde{q}_{ij}^{mn} = 0, \tag{56}$$

$$(\tilde{p}_{ij}^{m,n+1})^2 - (\tilde{p}_{ij}^{mn})^2 + \frac{\Delta_{ij}^x}{2}(\tilde{q}_{ij}^{mn}|\tilde{q}_{ij}^{mn}| + \tilde{q}_{ij}^{m,n+1}|\tilde{q}_{ij}^{m,n+1}|) = 0, \tag{57}$$

for all $P_{ij} \in \mathscr{P} - \mathscr{C}$, $0 \le m \le M$, and $0 \le n \le N-1$. By similar reasoning on pipes with compressors, we obtain (58)-(61) replacing (33)-(36):

$$\frac{\Delta_{ij}^x}{2}(\tilde{pt}_{iju}^{mn} + \tilde{pt}_{iju}^{m,n+1}) + \tilde{q}_{iju}^{m,n+1} - \tilde{q}_{iju}^{mn} = 0, \qquad 0 \le n \le k-1, \tag{58}$$

$$(\tilde{p}_{iju}^{m,n+1})^2 - (\tilde{p}_{iju}^{mn})^2 + \frac{\Delta_{ij}^x}{2}(\tilde{q}_{iju}^{mn}|\tilde{q}_{iju}^{mn}| + \tilde{q}_{iju}^{m,n+1}|\tilde{q}_{iju}^{m,n+1}|) = 0, \qquad 0 \le n \le k-1, \tag{59}$$

$$\frac{\Delta_{ij}^x}{2}(\tilde{pt}_{ijl}^{mn} + \tilde{pt}_{ijl}^{m,n+1}) + \tilde{q}_{ijl}^{m,n+1} - \tilde{q}_{ijl}^{mn} = 0, \qquad k \le n \le N-1, \tag{60}$$

$$(\tilde{p}_{ijl}^{m,n+1})^2 - (\tilde{p}_{ijl}^{mn})^2 + \frac{\Delta_{ij}^x}{2}(\tilde{q}_{ijl}^{mn}|\tilde{q}_{ijl}^{mn}| + \tilde{q}_{ijl}^{m,n+1}|\tilde{q}_{ijl}^{m,n+1}|) = 0, \qquad k \le n \le N-1 \tag{61}$$

for all $P_{ij} \in \mathscr{C}$ and $0 \le m \le M$. Overall, lumped element approximation can be seen as a simplified trapezoidal rule discretization in space, where (27) and (33)-(36) are omitted and (28), (38)-(41) are replaced with (56)-(57) and (58)-(61).

3.5. Constraints and Objective

We now show how to express the problem constraints and objective. The pressure variables must lie within the operational/safety bounds, as given in (8). In discretized form, we have for all $0 \le m \le M$ that

$$\underline{\tilde{p}}_{ij} \le \tilde{p}_{ij}^{nm} \le \overline{\tilde{p}}_{ij}, \qquad P_{ij} \in P - C, \quad 0 \le n \le N, \tag{62}$$

$$\underline{\tilde{p}}_{ij} \leq \tilde{p}^{nm}_{iju} \leq \overline{\tilde{p}}_{ij}, \qquad P_{ij} \in C, \quad 0 \leq n \leq k, \tag{63}$$

$$\underline{\tilde{p}}_{ij} \leq \tilde{p}^{nm}_{ijl} \leq \overline{\tilde{p}}_{ij}, \qquad P_{ij} \in C, \quad k \leq n \leq N \tag{64}$$

In addition, the compression ratio must lie within operational requirements and satisfy

$$\max\{\underline{R}_{ij}, 1\} \leq R^m_{ij} \leq \overline{R}_{ij}. \tag{65}$$

for all $P_{ij} \in \mathscr{C}$ and $0 \leq m \leq M$. The cost of compression is then expressed by a constraint

$$S^m_{ij} = \eta^{-1} \tilde{qm}^m_{ij}((R^m_{ij})^{2K} - 1) \tag{66}$$

for all $P_{ij} \in \mathscr{C}$ and $0 \leq m \leq M$, where $\tilde{qm}^m_{ij}$ is an auxiliary variable with the constraints

$$\tilde{qm}^m_{ij} \geq \tilde{q}^{mk}_{iju}, \quad \tilde{qm}^m_{ij} \geq -\tilde{q}^{mk}_{iju}, \tag{67}$$

so that minimizing $\tilde{qm}^m_{ij}$ will minimize $|\tilde{q}^{mk}_{iju}|$ (when $R^m_{ij} > 1$). Compressor cost is also constrained to be positive, i.e.,

$$S^m_{ij} \geq 0. \tag{68}$$

The balance conditions at junctions are enforced as follows. For all $0 \leq m \leq M$ and $J_j \in \mathscr{J}$,

$$\sum_{J_k \in \mathscr{J}: P_{jk} \in \mathscr{P}} \tilde{q}^{m0}_{jk} - \sum_{J_i \in \mathscr{J}: P_{ij} \in \mathscr{P}} \tilde{q}^{mN}_{ij} + \sum_{J_k \in \mathscr{J}: P_{jk} \in \mathscr{P}} \tilde{q}^{m0}_{jku} - \sum_{J_i \in \mathscr{J}: P_{ij} \in \mathscr{P}} \tilde{q}^{mN}_{ijl} = f^m_j, \text{ and} \tag{69}$$

For all $J_i, J_k \in \mathscr{J}$ s.t. $P_{ij}, P_{jk} \in \mathscr{P}$,

$$\tilde{p}^{mN}_{ij} = \tilde{p}^m_j = \tilde{p}^{m0}_{jk}. \tag{70}$$

Parametrization of these balance conditions for $0 \leq m \leq M$ is given by

$$f^m_i = \tilde{d}_i(t_m), \qquad J_i \in \mathscr{J} - \mathscr{S}, \tag{71}$$

$$p^m_i = \tilde{s}_i(t_m), \qquad J_i \in \mathscr{S}, \tag{72}$$

where $\tilde{d}_i(t)$ and $\tilde{s}_i(t)$ are given flow injection or supply pressure functions (in dimensionless form). The time-periodic boundary conditions on the states and controls are given for $0 \leq m \leq M$ by

$$-\varepsilon \leq \tilde{p}^{0n}_{ij} - \tilde{p}^{Mn}_{ij} \leq \varepsilon, \qquad \forall P_{ij} \in \mathscr{P} - \mathscr{C}, 0 \leq n \leq N \tag{73}$$

$$-\varepsilon \leq \tilde{p}^{0n}_{iju} - \tilde{p}^{Mn}_{iju} \leq \varepsilon, \qquad \forall P_{ij} \in \mathscr{C}, 0 \leq n \leq k \tag{74}$$

$$-\varepsilon \leq \tilde{p}^{0n}_{ijl} - \tilde{p}^{Mn}_{ijl} \leq \varepsilon, \qquad \forall P_{ij} \in \mathscr{C}, k \leq n \leq N \tag{75}$$

$$-\varepsilon \leq R^0_{ij} - R^M_{ij} \leq \varepsilon, \qquad \forall P_{ij} \in \mathscr{C}. \tag{76}$$

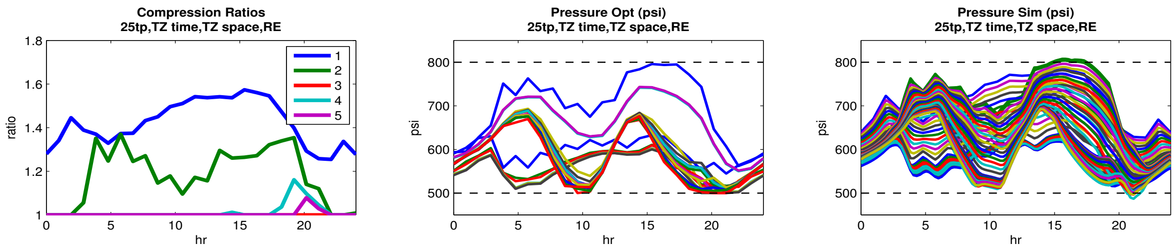

Figure 1 **A non-smooth solution with trapezoidal time and space discretization. Left to right: Compression ratios; Pressure trajectories (optimization); Pressure trajectories (simulation)**

where ε is a sufficiently small tolerance. The integral in the objective of problem (19) is approximated by a Riemann sum (normalized by U_m) of the form

$$C_1 \approx \sum_{P_{ij}\in\mathscr{C}} \sum_{m=0}^{M} U_m S_{ij}^m. \tag{77}$$

where U_m denotes weights for the compression energy at time point m. We set U_m to $2/(M+1)$ for trapezoidal time discretization and to $2\times w_m$ for pseudospectral time discretization to allow comparisons on the objective values for both discretization on the same scale (i.e. the dimensionless time interval re-scaled to $[-1,1]$).

4. The Two-Stage Optimization Model

A direct encoding of the optimization problem over the discretized constraints and objectives may result in solutions where the pressure, flow, and compression ratio solutions may not be smooth. Figure 1 exhibits such a behavior on one of our test cases. The left and middle subfigures depict the compressor ratios and the pressures obtained by such a direct encoding. The right figure shows the results of a dynamic adaptive simulation using the optimal compressor ratios. The rapidly changing compression ratios in the optimal solution are undesirable from an operational standpoint: The application of such non-smooth controls would result in fast changes in pressure and flux (as seen in the right subfigure in Figure 1) which may cause severe damage to turbomachinery or piping. Moreover, the jitters in the pressure trajectories (in the middle subfigure) indicates that the physics is not represented accurately. Finally, the simulated pressures for these compressor ratios also violate their bounds and raises potential safety issues in practice.

To remedy these limitions, we add a second objective function that aims at producing smooth compressor ratios. This second objective minimizes

$$C_2 = \sum_{P_{ij}\in\mathscr{C}} \sum_{m=0}^{M} \left[\frac{\partial^2 R_{ij}^m}{\partial \tilde{t}_{ij}^2}\right]^2 \tag{78}$$

i.e., the sum of the second derivatives of the compressor ratios over time. For the trapezoidal time discretization, the second derivatives can be approximated by

$$\frac{\partial^2 R_{ij}^m}{\partial \tilde{t}_{ij}^2} \approx (R_{ij}^{m+1} - R_{ij}^m) - (R_{ij}^m - R_{ij}^{m-1}) = R_{ij}^{m+1} + R_{ij}^{m-1} - 2R_{ij}^m$$

where we map R_{ij}^{-1} to R_{ij}^{M-1} and R_{ij}^{M+1} to R_{ij}^1 for the boundary cases. For the pseudospectral time discretization, we use

$$\frac{\partial^2 R_{ij}^m}{\partial \tilde{t}_{ij}^2} \approx \sum_{g=0}^{M} \frac{2}{\tilde{T}_{ij}} D_{mg}^2 R_{ij}^g$$

where D^2 is equal to the matrix product of the differential matrix D with itself (i.e., $D^2 = D \cdot D$).

To integrate the two objectives, we employ a lexicographic strategy in our implementation. We first solve the original nonlinear program with the first objective (77), and then solve the nonlinear program with the second objective (78), while imposing the additional constraint

$$C_1 \leq (1+r)f, \text{ where } 0 \leq r \leq 1 \tag{79}$$

where f is the objective value obtained from the first step. Intuitively, the tolerance r is a user-adjustable parameter that quantifies the factor of increase in compression energy that can be traded for a smoother solution. In our implementation, the second stage is initialized with the first-stage solution. This two-stage approach had the desirable property that smoothness can really be controlled effectively, which was not the case when using a weighted sum of the two objectives with a penalty on C_2 or when imposing a smoothness-enforcing constraint directly in a one-stage optimization model. We now summarize our formulation. The first-stage optimization is specified by

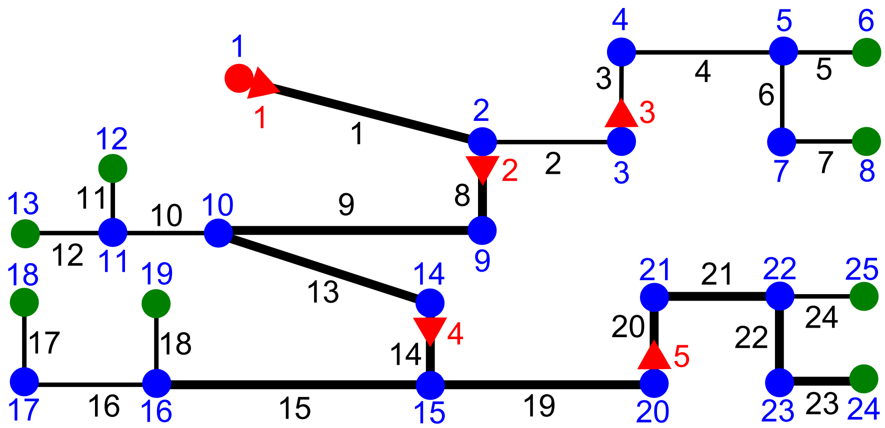

Figure 2 **24-pipe gas system test network used in the benchmark case study. Numbers indicate nodes (blue), edges (black), and compressors (red). Thick and thin lines indicate 36 and 25 inch pipes. Nodes are source (red), transit (blue), and consumers (green).**

$$
\begin{aligned}
&\min\ C_1 : (77)\\
&s.t.\ \ \text{time dynamics, either:} \begin{cases}\text{Trapezoidal: } (26), (31)-(32), \text{ or}\\ \text{Pseudospectral: } (49), (50)-(51)\end{cases}\\
&\qquad\ \text{space dynamics, either:} \begin{cases}\text{Trapezoidal: } (27), (28), (33)-(36), (38)-(41), \text{ or}\\ \text{Lumped element: } (56)-(61)\end{cases}\\
&\qquad\ \text{Pressure \& compression safety constraints: } (62)-(65)\\
&\qquad\ \text{compressor power: } (66)-(68)\\
&\qquad\ \text{junction conditions: } (37), (69)-(70)\\
&\qquad\ \text{boundary parameters: } (71)-(72)\\
&\qquad\ \text{periodicity constraints: } (73)-(76)
\end{aligned}
\tag{80}
$$

while the second-stage optimization is given by

$$
\begin{aligned}
&\min\ C_2 : (78)\\
&s.t.\ \ \text{1st stage problem constraints: } (80)\\
&\qquad\ \text{Solution tolerance: } (79)
\end{aligned}
\tag{81}
$$

5. Case Studies

The large-scale nonlinear programs for our DOGF problems are modeled with AMPL (version 2014) [50, 51] and solved with the nonlinear solver IPOPT 3.12.2, ASL routine (version 2015) [41] with AMPL pre-solve. The implementation is run on a Dell PowerEdge R415 with AMD Opteron

4226 and 64 GB of ram. We present the computational results of three case studies that include a validation of the approach, as well as results about solution quality, efficiency, and scalability.

5.1. Validation

The solution obtained using our implementation was validated on the 24-pipe benchmark gas network used in prior work [34], and illustrated in Figure 2. The pressures at supply sources were fixed at 500psi ($\approx 3.45 \times 10^6$ Pa), the dimensionless constants for the dimensionless equation transformation were set to p_N = 250psi ($\approx 1.72 \times 10^6$ Pa) and q_N = 100 kg/s, physical parameters a = 377.968 m/s, $\gamma = 2.5$, and $\lambda = 0.01$ were used, and a time horizon $T = 24$ hrs (86400s) was considered. Parameters $D_{ij}, A_{ij}, L_{ij}, \overline{R_{ij}}$, and $\underline{R_{ij}}$ were set according to the benchmark case study, as well as time-dependent profiles of gas injections/withdrawals $d_i(t)$. The benchmark network structure and the gas draw profiles are provided in the online supplement section. For the trapezoidal space approximation, each pipe P_{ij} is discretized uniformly according to its length L_{ij} into $\lceil L_{ij}/E \rceil + 1$ segments, where E is set to 10km by default. The test case is a tree network and hence the flow direction on each pipe is known. The compressors are placed on the first segment of the i^{th} end of every pipe $P_{ij} \in \mathscr{C}$.

The admissible pressure range is 500 to 800 psi throughout the network. A feasible solution to the discretized problem that satisfies the pressure constraints may cause these constraints to be violated in a high-accuracy simulation of the dynamics for the continuous problem. To address this issue, one version of our implementation tightens the pressure bounds conservatively by 4% or less, i.e., in the range [520,780] psi for this particular benchmark. We refer to this as “tightened” problem, while optimizing over the nominal constraints of 500 to 800 psi is referred to as the “regular” problem.

The optimization results were validated by using the optimized compression ratio solution as a time-varying parameter in a validated dynamic simulation method [42, 43]. The trajectories computed using the simulation are used to validate the optimization solution in two ways. First, we quantify how much the constraints on pressure are exceeded by evaluating the L_2-norm of the violations. The violation measure aggregates violations over the 24-hour period by integrating the square of the pressure violations (psi) of the bounds at every junction. It is defined by

$$v_p = \sqrt{\sum_{P_{ij} \in \mathscr{P}} [\int_0^T (p_{ij}(t,0) - p_{\max})_+ \mathrm{d}t + \int_0^T (p_{\min} - p_{ij}(t, L_{ij}))_+ \mathrm{d}t]^2} \tag{82}$$

Table 1 Aggregated Pressure Bound Violations (v_p, psi-days): 24 Pipe. (simulation: 10km space discretization)

	Trapezoidal time - trapezoidal space				Trapezoidal time - lumped element space			
Bounds	Tightened		Regular		Tightened		Regular	
Time pt.	5%	10%	5%	10%	5%	10%	5%	10%
25tp	0.000	0.000	0.913	0.899	0.000	0.000	0.939	0.876
50tp	0.000	0.000	0.076	0.058	0.000	0.000	0.116	0.090
100tp	0.000	0.000	0.000	0.007	0.000	0.000	0.000	0.000
200tp	0.000	0.000	0.004	0.000	0.000	0.000	0.000	0.000
	Pseudospectral time - trapezoidal space				Pseudospectral time - lumped element space			
Bounds	Tightened		Regular		Tightened		Regular	
Time pt.	5%	10%	5%	10%	5%	10%	5%	10%
25tp	0.000	0.000	0.451	0.205	0.000	0.000	0.186	0.059
50tp	0.000	Time Limit	0.026	0.026	0.000	0.000	0.000	0.021

Table 2 Aggregated Pressure Bound Violations (v_p, psi-days): 24 Pipe. (simulation: 3km space discretization)

	Trapezoidal time - trapezoidal space				Trapezoidal time - lumped element space			
Bounds	Tightened		Regular		Tightened		Regular	
Time pt.	5%	10%	5%	10%	5%	10%	5%	10%
25tp	0.000	0.000	0.951	0.916	0.000	0.000	0.994	0.896
50tp	0.000	0.000	0.100	0.071	0.000	0.000	0.146	0.109
100tp	0.000	0.000	0.000	0.001	0.000	0.000	0.000	0.000
200tp	0.000	0.000	0.000	0.000	0.000	0.000	0.000	0.000
	Pseudospectral time - trapezoidal space				Pseudospectral time - lumped element space			
Bounds	Tightened		Regular		Tightened		Regular	
Time pt.	5%	10%	5%	10%	5%	10%	5%	10%
25tp	0.000	0.000	0.404	0.175	0.000	0.000	0.162	0.037
50tp	0.000	Time Limit	0.020	0.019	0.000	0.000	0.000	0.035

where $(x)_+ = x$ if $x \geq 0$ and $(x)_+ \equiv 0$ if $x < 0$. The unit of the metric is psi-days. Tables 1 and 2 list solution values found using various time discretizations, smoothing parameter r, the tightened vs. regular problems, and using 3km and 10km space discretization settings. With tightened bounds, the optimization solution has no, or negligible, violations in the studied configurations.

Figure 3 depicts the optimal compressor ratio functions for 25 and 200 trapezoidal time discretization, 25 and 50 pseudospectral time discretization, with tightened and regular constraints, respectively, and with $E = 10$km spatial trapezoidal discretization and lumped element approximation. The second-stage tolerance r is set to 5%. The results show that the compressor ratios over time are smooth, producing meaningful physical solutions and control profiles that can be implemented by operators. This is true even for coarse time discretizations. The only exception is the pseudo-spectral discretization (25tp, PS time, TZ space, 5%, tightened).

Table 3 Maximum relative difference (%) in pressure between simulation and optimization: 24 Pipe (simulation: 10km space discretization)

	Trapezoidal time - trapezoidal space				Trapezoidal time - lumped element space			
Bounds	Tightened		Regular		Tightened		Regular	
Time pt.	5%	10%	5%	10%	5%	10%	5%	10%
25tp	3.560	2.974	3.642	3.408	3.410	5.756	5.641	3.413
50tp	1.935	2.668	1.503	2.767	2.721	3.350	3.302	2.431
100tp	2.062	2.480	2.126	1.723	1.883	3.500	2.137	2.923
200tp	1.412	1.335	1.248	1.314	1.291	1.499	1.267	1.399
	Pseudospectral time - trapezoidal space				**Pseudospectral time - lumped element space**			
Bounds	Tightened		Regular		Tightened		Regular	
Time pt.	5%	10%	5%	10%	5%	10%	5%	10%
25tp	3.936	4.777	4.107	4.785	3.861	4.767	4.001	4.694
50tp	0.922	Time Limit	1.004	0.950	0.734	0.795	0.806	0.756

The last column of Figure 3 describes validation results that compare the optimization solutions with simulations. The simulation results were found by providing the optimal control solutions as input to a dynamic simulation of a differential algebraic equation (DAE) model of the network [34] and the adaptive time-stepping solver `ode15i` in MATLAB. Figure 3 reports the relative difference between the optimized pressure profiles p_j^m (re-scaled from dimensionless to nominal unit) for every junction in the network with the pressure trajectories $p_j^{m\star}$ obtained from simulations over time. Table 3 and Table 4 give the maximum relative error (in %) across all the pipe junctions and all the time steps for our four discretization schemes with the formula:

$$\max_{0 \le m \le M} \; [\max_{J_j \in \mathscr{J}} (|\frac{p_j^m - p_j^{m\star}}{p_j^m}|)] \times 100\% \tag{83}$$

We tested the test cases with both regular and tightened constraints, with a 5% and 10% re-optimization tolerance, and with both 3km and 10km space discretization settings in simulations.

With only 25 time points, the (time and space) trapezoidal methods gave smooth control profiles with less than 4% of error when compared with simulations. This error disappears almost entirely with 200 time points. In general, the lumped element method with a trapezoidal discretization for time gives slighly less accurate results.

Because the sources of the compared pressure profiles are qualitatively very different, i.e., optimization of algebraic equations that discretize PDEs over a fixed grid compared with adaptive time-stepping solution of an ODE system, these results are a powerful cross-validation of both models.

Table 4 Maximum relative difference (%) in pressure between simulation and optimization: 24 Pipe (simulation: 3km space discretization)

	Trapezoidal time - trapezoidal space				Trapezoidal time - lumped element space			
Bounds	Tightened		Regular		Tightened		Regular	
Time pt.	5%	10%	5%	10%	5%	10%	5%	10%
25tp	3.584	3.014	3.732	3.443	3.420	5.744	5.625	3.451
50tp	1.937	2.591	1.537	2.697	2.658	3.285	3.330	2.340
100tp	2.047	2.391	2.037	1.618	1.833	3.377	2.167	2.906
200tp	1.357	1.225	1.222	1.268	1.251	1.391	1.274	1.365
	Pseudospectral time - trapezoidal space				Pseudospectral time - lumped element space			
Bounds	Tightened		Regular		Tightened		Regular	
Time pt.	5%	10%	5%	10%	5%	10%	5%	10%
25tp	3.928	4.765	4.049	4.716	3.807	4.772	3.990	4.584
50tp	0.957	Time Limit	0.996	0.951	0.743	0.738	0.776	0.761

5.2. Solution Quality and Efficiency

Table 5 reports the objective value C_1, computation time, and the number of variables of the proposed method for: a) trapezoidal time, trapezoidal space discretization, b) trapezoidal time, lumped element space discretization, c) pseudospectral time, trapezoidal space discretization, and d) pseudospectral time, lumped element space discretization, with smoothness parameters r equals to 5% and 10%. We vary time points from 25pt up to 300pt/50tp for trapezoidal/pseudospectral time discretization respectively. The table gives the value of the C_1 objective after the first stage, and also in the second stage for $r = 5\%$ and 10%. CPU times in seconds reported by IPOPT for the first and second stages are also given. First, observe that enforcing the smoothness of the solution does not fundamentally decrease the quality of the C_1 objective, which is important from an operational standpoint. Second, as expected, refining the time discretization increases the objective value in the various trapezoidal schemes (since more constraints are added). Third, for the trapezoidal time discretization, the convergence rate is fast and the solutions obtained with a coarse discretization are already of high quality, as illustrated in Figure 3. The lumped element approximation further reduces the model size by more than 50% and increases computational efficiency by factors from 4 to 25 depending on the accuracy of the discretization. As a result, the method exhibits excellent performance. Consider the time granularities with 25 and 50 points: For $r = 10\%$, the method requires less than 10 seconds, which indicates that it can be used during real-time operations. On the other hand, the pseudospectral time discretizations are orders of magnitude slower than trapezoidal scheme. Pseudospectral methods link every pressure/flux differential variable to pressure/flux variables at every time step [47, 49], producing a dense constraint matrix. Since the

Table 5 Objective Value (C_1) and runtimes on 24 Pipe Network.

	Trapezoidal time - trapezoidal space discretization							Trapezoidal time - lumped element space discretization						
	Var. no.	Objective Value			CPU Time (secs)			Var. no.	Objective Value			CPU Time (secs)		
		1st Stage	2nd Stage		1st Stage	2nd Stage			1st Stage	2nd Stage		1st Stage	2nd Stage	
			$r = 5\%$	10%		$r = 5\%$	10%			$r = 5\%$	10%		$r = 5\%$	10%
25tp	11441	2.012	2.112	2.213	12	22	8	4785	2.003	2.103	2.203	3	5	3
40tp	18041	2.088	2.193	2.297	35	78	22	7545	2.068	2.172	2.275	6	12	6
50tp	22441	2.073	2.176	2.280	32	75	28	9385	2.069	2.172	2.276	9	21	10
60tp	26841	2.091	2.195	2.300	43	164	42	11225	2.088	2.192	2.297	25	29	10
80tp	35641	2.106	2.211	2.316	45	208	55	14905	2.096	2.201	2.306	22	49	23
100tp	44441	2.126	2.233	2.339	131	230	73	18585	2.100	2.205	2.310	65	80	32
150tp	66441	2.105	2.210	2.316	266	800	280	27785	2.105	2.210	2.315	163	335	86
200tp	88441	2.136	2.243	2.350	545	582	447	36985	2.114	2.220	2.325	320	299	145
300tp	132441	2.136	2.243	2.349	32169	2028	639	55385	2.115	2.221	2.327	1212	309	345

	Pseudospectral time - trapezoidal space discretization							Pseudospectral time - lumped element space discretization						
	Var. no.	Objective Value			CPU Time (secs)			Var. no.	Objective Value			CPU Time (secs)		
		1st Stage	2nd Stage		1st Stage	2nd Stage			1st Stage	2nd Stage		1st Stage	2nd Stage	
			$r = 5\%$	10%		$r = 5\%$	10%			$r = 5\%$	10%		$r = 5\%$	10%
25tp	11389	2.168	2.276	2.384	337	572	435	4759	2.161	2.270	2.378	72	185	126
50tp	22339	2.114	2.219	2.325	17160	31882	46687	9334	2.147	2.255	2.362	14309	30535	29836

iteration counts of IPOPT for both types of discretization are similar in scale, the increased matrix density in the pseudospectral discretization is responsible for the observed loss in efficiency.

5.3. Scalability

To study the scalability of the proposed method, two additional instances are considered: Gaslib-40 and Gaslib-135 from the GasLib library [52]. The pressure ranges are set to 500 to 800 psi and 500 to 1000 psi for Gaslib-40 and Gaslib-135 respectively, and the source pressures are set to 600 psi. Tables 6–8 present the results on solution quality and efficiency. We omit results for pseudospectral time method since it does not converge or scales poorly on both benchmarks.

The trapezoidal time methods scale well on Gaslib-40 and they exhibit similar behavior as in the 24-pipe network. In particular, it can be solved in less than two minutes. The Gaslib-135 network is much more challenging and consists of more than 6000km of pipes. Hence, we only consider the lumped element method and relax the acceptable tolerances (termination condition) of IPOPT from 10^{-6} to 10^{-4} given the size of the test case. The cases that satisfy the acceptable tolerance but fail to reach the optimality region (IPOPT default: 10^{-8}) are marked with '$*'$ in the objective column. The results show that the lumped element method finds high-quality solutions in reasonable time, solving a 25pt discretization in about an hour. The objective function does not necessarily increase monotonically due to the difficulty in reaching the feasibility region. Still these results are promising and demonstrate the method's ability to find high-quality solutions to large networks.

Table 6 Objective Value (C_1) and runtimes on Gaslib-40 Pipe Network.

	Trapezoidal time - trapezoidal space discretization							Trapezoidal time - lumped element space discretization						
	Var. no.	Objective Value 1st Stage	2nd Stage		CPU Time (secs) 1st Stage	2nd Stage		Var. no.	Objective Value 1st Stage	2nd Stage		CPU Time (secs) 1st Stage	2nd Stage	
			$r = 5\%$	10%		$r = 5\%$	10%			$r = 5\%$	10%		$r = 5\%$	10%
20tp	20707	0.260	0.273	0.286	191	28	24	6910	0.254	0.267	0.279	51	4	4
30tp	30567	0.294	0.309	0.323	541	54	268	10200	0.297	0.312	0.326	45	40	39
40tp	40427	0.297	0.312	0.327	1143	164	444	13490	0.310	0.326	0.341	142	61	90
50tp	50287	0.311	0.326	0.342	1316	213	1513	16780	0.311	0.326	0.342	148	84	153
100tp	99587	0.321	0.337	0.353	9395	2666	1953	33230	0.322	0.339	0.355	2566	648	575
150tp	148887	0.323	0.339	0.355	15171	9363	8003	49680	0.325	0.342	0.358	5139	3309	2605

Table 7 Maximum relative difference (%) in pressure between simulation and optimization: Gaslib-40

	Trapezoidal time & trapezoidal space		Trapezoidal time & lumped element space	
Time pt.	5%	10%	5%	10%
20tp	6.198	–	5.705	4.086
50tp	1.835	1.773	2.119	2.068
100tp	3.915	3.878	3.832	3.864
150tp	3.381	3.422	3.362	3.403

Table 8 Objective Value (C_1) and runtimes on Gaslib-135 Pipe Network.

	Trapezoidal time - lumped element space discretization						
	Var. no.	Objective Value 1st Stage	2nd Stage		CPU Time (secs) 1st Stage	2nd Stage	
			$r = 5\%$	10%		$r = 5\%$	10%
15tp	18769	2.027*	2.128	2.229	598	112	117
20tp	24634	2.492*	2.617	2.741*	713	314	445
25tp	30499	2.203*	2.313	2.423	1788	330	236

We also report results on the validation of the solutions for Gaslib-40. Figure 4 presents the pressure and flow profiles resulting from simulations. The figure shows the differences in percentage for each junction over time between optimization and simulation on pressure trajectories. Table 7 again shows the maximum relative error across all the pipe junctions. In this larger benchmark, the method produces smooth control profiles with less than 2% of error using 50 trapezoidal time points. Figure 5 further shows two compression solutions on the Gaslib-135 benchmark.

The results in Figures 3–4 also show the benefits and justify our two-stage approach. The figures demonstrate that the largest errors occur when there are fast changes in the demands and are not due to compressor ratios.

5.4. Extensions & Variants

We now present a related optimization problem to showcase the generality of the dynamic gas pipeline flow modeling proposed here. With the growing number of gas-fired generators, it becomes important in planning and signing contracts to understand how much gas could be supplied, packed into the system, and delivered to potential customers at any time. It is also important to understand the bottlenecks of transmission networks when planning for future upgrades.

In this section, we modify our optimization problem for the 24-pipe system to maximize the outflows for a set of important demand points $\mathscr{D} \subseteq \mathscr{J}$, while keeping the flow profiles for the other demands $\mathscr{J} \setminus \mathscr{D}$ fixed. In other words, equation (71) will be relaxed for demands in $\mathscr{D}$. To align our experiments with industry practice, we seek the maximal outflows that are steady (i.e., constant over time). Thus, we create decision variables f_j for functions $J_j \in \mathscr{D}$ and change (69) for these junctions to

$$\sum_{J_k \in \mathscr{J}:P_{jk} \in \mathscr{P}} \tilde{q}_{jk}^{m0} - \sum_{J_i \in \mathscr{J}:P_{ij} \in \mathscr{P}} \tilde{q}_{ij}^{mN} + \sum_{J_k \in \mathscr{J}:P_{jk} \in \mathscr{P}} \tilde{q}_{jku}^{m0} - \sum_{J_i \in \mathscr{J}:P_{ij} \in \mathscr{P}} \tilde{q}_{ijl}^{mN} = f_j, \quad f_j <= 0 \tag{84}$$

where f_j is now steady. We then replace (77) by

$$\max M_1 = -\sum_{J_j \in \mathscr{D}} c_j f_j \tag{85}$$

where c_j is the node-dependent costs. We further add penalty terms in (78) to smooth the source flux $\mathscr{S}$ which act as the slack variable in our formulation. This gives

$$C_2 = \sum_{P_{ij} \in \mathscr{C}} \sum_{m=0}^{M} \left[\frac{\partial^2 R_{ij}^m}{\partial \tilde{t}_{ij}^2} \right]^2 + w_p \sum_{J_j \in \mathscr{S}} \sum_{m=0}^{M} \left[\frac{\partial^2 f_j^m}{\partial t^2} \right]^2 \tag{86}$$

where w_p is the weight of the new penalty and f_j^m are the flux variables of the source. We use the same method as in (78) to approximate the second derivatives of f_j^m for both the trapezoidal and pseudospectral discretizations. Because we switch from minimization to maximization, we flip the inequality in (79) to obtain:

$$M_1 \geq (1-r)v, \text{ where } 0 \leq r \leq 1, \tag{87}$$

and where v is the objective value obtained in the first step.

We report experimental results on on the 24 pipe system with three different cases:

1. Maximizing the outflow integral of 5 nodes with equal costs: $c_j = 1$ and $\mathscr{D} = \{6, 8, 12, 13, 19\}$,
2. Maximizing outflow of only node 19: $c_j = 1$ and $\mathscr{D} = \{19\}$, and
3. Case 1 with different weights/preferences c_j as shown in Table 9.

Table 9 Gas price ($ per 10 kg mass) and optimized demand (kg/s).

Trapezoidal time, lumped space, 50 time point, $r = 7\%$			
Node number	Gas price	Demand (case 1)	Demand (case 3)
6	1.0	21.582	0.000
8	1.5	16.498	36.067
12	2.0	87.537	38.836
13	2.0	0.057	0.025
19	3.0	0.000	46.364

5.4.1. Case 1. Table 10 shows the model size, objective values M_1, and computational runtimes for our 4 different discretization schemes on case 1 with varying number of time points and with two re-optimization tolerances: $r = 3\%$ and 7%. The smoothness weighting w_p is set to 50. Figures 6 and 7 depict the demand, as well as the compression ratio, the pressure and the flux at each junction point, the relative error (in %) between simulation and optimization, and the optimized maximum demands on one of the settings: 50 trapezoidal time points with lumped element discretization in space. We obtain similar results to those of Sections 5.2–5.3. At the coarser discretization, the error between optimization and simulation is approximately 2%. The convergence rate is fast for the trapezoidal time discretization and the solutions obtained with a coarse discretization are already of high quality. The lumped element approximation once again decreases the size of the model and improves the computational efficiency significantly. The pseudospectral time discretization is still orders of magnitude slower than the trapezoidal schemes.

Observe that the solution tends to allocate more flux for node 12 (refer to Figure 6/Table 9), located in the top-left portion of the 24-pipe network (see Figure 2), when compared to the other regions (e.g. the top-right and bottom-left regions). The path between the source at node 1 to node 11 consists of: a) a total of 165 km of three 36” diameter pipes, and b) one 5 km long 25” diameter pipe. If we roughly estimate resistance based on distance divided by diameter (in the unit of km/m), this will give a resistance metric of 188 (km/m). The path between the source at node 1 to node 5 consists of: a) one 100 km long 36” diameter pipe, and b) a total of 50km of three 25” diameter pipes. This will also give a resistance metric of 188 (km/m). However, the pipe length of pipe 11 (or 12) is slightly shorter than pipe 5 (or the combined length of pipe 6 and 7). This results in a lower resistance for allocating flux to the top-left region than the top-right region. Since we aim at minimizing compression energy for all of the compressors, the optimization model naturally chooses to optimize the path of least resistance (for compressor 2). Allocating flux to the path with more resistance would incur more compression energy (on compressor 3).

Table 10 Objective Value (M_1) and runtimes on the maximum contractable throughput model: case 1

	Trapezoidal time - trapezoidal space discretization							Trapezoidal time - lumped element space discretization						
	Var. no.	Objective Value 1st Stage	Objective Value 2nd Stage		CPU Time (secs) 1st Stage	CPU Time (secs) 2nd Stage		Var. no.	Objective Value 1st Stage	Objective Value 2nd Stage		CPU Time (secs) 1st Stage	CPU Time (secs) 2nd Stage	
			$r = 3\%$	7%		$r = 3\%$	7%			$r = 3\%$	7%		$r = 3\%$	7%
25tp	11576	1.366	1.325	1.271	5	7	4	4920	1.362	1.322	1.267	3	1	1
50tp	22701	1.356	1.315	1.261	25	17	36	9645	1.351	1.311	1.257	12	5	7
100tp	44951	1.349	1.309	1.255	118	202	86	19095	1.345	1.304	1.251	88	21	26
200tp	89451	1.348	1.308	1.254	1735	196	323	37995	1.345	1.304	1.251	1017	143	248
	Pseudospectral time - trapezoidal space discretization							Pseudospectral time - lumped element space discretization						
	Var. no.	Objective Value 1st Stage	Objective Value 2nd Stage		CPU Time (secs) 1st Stage	CPU Time (secs) 2nd Stage		Var. no.	Objective Value 1st Stage	Objective Value 2nd Stage		CPU Time (secs) 1st Stage	CPU Time (secs) 2nd Stage	
			$r = 3\%$	7%		$r = 3\%$	7%			$r = 3\%$	7%		$r = 3\%$	7%
25tp	11524	1.341	1.301	1.247	297	162	215	4894	1.350	1.309	1.255	112	141	186
50tp	22599	1.352	1.312	1.258	33446	20305	17780	9594	1.348	1.308	1.254	8262	13710	11775

5.4.2. Cases 2 and 3. Case 2 is essentially a simplification of case 1, with the goal of finding the maximum contractable throughput for a specific demand point in the presence of the remaining known load profiles. Case 3 further considers price weights among different demands, with the goal to find the optimal contractable throughput based on maximum revenue to the pipeline operator. The optimal solution will then represent the maximum contractable revenue that the gas transmission system can obtain by optimizing allocation of supplies to flexible customers with different offer bids. We repeat the computational studies as done in previous sections on both cases with the trapezoidal time discretization and the lumped element space approximation. Table 11 shows the model size, objective values M_1, and computational runtimes. Figure 6 and Table 9 present one of the solutions and compare it with case 1. Figures 7 and 8 also show the compression ratio, the pressure, and the flux at each junction point, and the relative error (in %) between simulation and optimization for 50 time points. Once again, the results are consistent with the earlier case studies. The errors could be further reduced by increasing the discretization to 200 time points (Figure 8). Overall, these results show that the proposed method produces consistent results across a number of case studies and objectives.

6. Conclusions

This paper investigated the Dynamic Optimal Gas Flow (DOGF) problem of pipeline flow management whose goal is to minimize compressor operating costs while maintaining pressure constraints under dynamic intra-day conditions where offtakes by customers are described by time-dependent mass flow functions. This study was motivated by the growing reliance of electric power systems on

Table 11 Objective Value (M_1) and runtimes: case 2 and 3

	Case 2							Case 3						
	Var. no.	Objective Value			CPU Time (secs)			Var. no.	Objective Value			CPU Time (secs)		
		1st Stage	2nd Stage		1st Stage	2nd Stage			1st Stage	2nd Stage		1st Stage	2nd Stage	
			$r = 3\%$	7%		$r = 3\%$	7%			$r = 3\%$	7%		$r = 3\%$	7%
25tp	4812	0.727	0.705	0.676	3	1	1	4920	2.955	2.867	2.748	3	2	1
50tp	9437	0.704	0.683	0.654	7	4	5	9645	2.913	2.826	2.709	12	4	5
100tp	18687	0.695	0.674	0.647	51	22	13	19095	2.892	2.805	2.689	59	24	24
200tp	37187	0.696	0.675	0.647	500	178	330	37995	2.893	2.807	2.691	359	89	180

gas-fired generation, which has been driven by the need to balance intermittent sources of renewable energy and low prices for new power plant construction and natural gas. This deeper integration has increased the variation and volume of flows through natural gas transmission pipelines, making progress beyond steady-state optimization a critical operational need for controlling and optimizing natural gas networks. Maintaining efficiency and security under such dynamic conditions requires optimization methods that accurately account for intra-day transients and can quickly compute solutions to follow generator re-dispatch.

This paper presented an efficient scheme for the DOGF that relies on a compact yet appropriately accurate representation of gas flow physics. The paper also detailed two time- and two space-discretization methods and formalized the nonlinear model for optimization. A two-stage approach is applied to minimize energy costs and maximize smoothness of compressor ratios to obtain physically realistic solutions. The resulting large-scale nonlinear programs are solved using a general interior-point method, and the results are validated against an accurate simulation of the dynamic equations and a recently proposed state-of-the-art method. The novel optimization scheme yields solutions that are feasible for the continuous problem and practical from an operational standpoint. Scalability of the scheme was demonstrated using three networks with 25, 40, and 135 nodes, 24, 45, and 170 pipes, and total pipeline lengths of 477, 1118, and 6964 kilometers respectively. We further extended the formulation to tackle the maximum throughput problem, demonstrating the flexibility of our model. This opens new directions for the investigation of previously computationally difficult control and optimization problems involving gas networks, as well as integration of pipeline operations with electric power systems.

References

[1] M. Qadrdan, M. Chaudry, J. Wu, N. Jenkins, and J. Ekanayake. Impact of a large penetration of wind generation on the gb gas network. *Energy Policy*, 38(10):5684–5695, 2010.

[2] P. J. Hibbard and T. Schatzki. The interdependence of electricity and natural gas: current factors and future prospects. *The Electricity Journal*, 25(4):6–17, 2012.

[3] C. Lyons and G. Litra. Gas-power interdependence: Knock-on effects of the dash to gas, 2013. `http://www.scottmadden.com/insight/598/gaspower-interdependence.html`.

[4] T. Li, M. Eremia, and Mohammad Shahidehpour. Interdependency of natural gas network and power system security. *Power Systems, IEEE Transactions on*, 23(4):1817–1824, 2008.

[5] Richard Schmalensee. Growing concerns, possible solutions: The interdependency of natural gas and electricity systems. Technical report, MIT Energy Initiative, April 2013. `http://energy.mit.edu/publication/growing-concerns-possible-solutions/`.

[6] M. Chertkov, S. Backhaus, and V. Lebedev. Cascading of fluctuations in interdependent energy infrastructures: Gas-grid coupling. *Applied Energy*, 160:541 – 551, 2015.

[7] R. D. Tabors and S. Adamson. Measurement of energy market inefficiencies in the coordination of natural gas &; power. In *47th Hawaii International Conference onSystem Sciences (HICSS)*, pages 2335–2343. IEEE, 2014.

[8] R. Z. Ríos-Mercado and C. Borraz-Sánchez. Optimization problems in natural gas transportation systems: A state-of-the-art review. *Applied Energy*, 147:536–555, 2015.

[9] Thorsten Koch, Benjamin Hiller, Marc E Pfetsch, and Lars Schewe. *Evaluating gas network capacities*. SIAM, 2015.

[10] P. Wong and R. Larson. Optimization of natural-gas pipeline systems via dynamic programming. *Automatic Control, IEEE Transactions on*, 13(5):475–481, 1968.

[11] B. Rothfarb, H. Frank, D. M. Rosenbaum, K. Steiglitz, and D. J. Kleitman. Optimal design of offshore natural-gas pipeline systems. *Operations research*, 18(6):992–1020, 1970.

[12] K. T. Midthun, M. Bjørndal, and A. Tomasgard. Modeling optimal economic dispatch and system effects in natural gas networks. *The Energy Journal*, pages 155–180, 2009.

[13] C. Borraz-Sanchez. *Optimization methods for pipeline transportation of natural gas*. PhD thesis, Bergen Univ.(Norway), 2010.

[14] S. Misra, M. W. Fisher, S. Backhaus, R. Bent, M. Chertkov, and F. Pan. Optimal compression in natural gas networks: A geometric programming approach. *IEEE Transactions on Control of Network Systems*, 2(1):47–56, 2015.

[15] F. Babonneau, Y. Nesterov, and J.-P. Vial. Design and operations of gas transmission networks. *Operations research*, 60(1):34–47, 2014.

[16] C. Borraz-Sanchez, R. Bent, S. Backhaus, H. Hijazi, and P. Van Hentenryck. Convex relaxations for gas expansion planning. *INFORMS Journal on Computing*, to be published.

[17] R. Levitan, S. Wilmer, and R. Carlson. Pipeline to reliability: Unraveling gas and electric interdependencies across the eastern interconnection. *Power and Energy Magazine, IEEE*, 12(6):78–88, 2014.

[18] G. L. Peters. Gas and electric infrastructure interdependency analysis. *Envision Energy Solutions*, 22, 2012.

[19] G. L. Peters. Embedded natural gas-fired electric power generation infrastructure analysis: An analysis of daily pipeline capacity availability. Technical report, EnVision Energy Solutions, 2012.

[20] M. Chertkov, M. Fisher, S. Backhaus, R. Bent, and S. Misra. Pressure fluctuations in natural gas networks caused by gas-electric coupling. In *2015 48th Hawaii International Conference on System Sciences (HICSS)*. IEEE, 2015.

[21] M. Shahidehpour and Z. Li. White paper: Long-term electric and natural gas infrastructure requirements. Technical report, Illinois Institute of Technology, 2014.

[22] A. Osiadacz. Simulation of transient gas flows in networks. *International journal for numerical methods in fluids*, 4(1):13–24, 1984.

[23] M. Herty, J. Mohring, and V. Sachers. A new model for gas flow in pipe networks. *Mathematical Methods in the Applied Sciences*, 33(7):845–855, 2010.

[24] A. D. Woldeyohannes and M. A. Majid. Simulation model for natural gas transmission pipeline network system. *Simulation Modelling Practice and Theory*, 19(1):196–212, 2011.

[25] D. Matko, G. Geiger, and W. Gregoritza. Verification of various pipeline models. *Mathematics and computers in simulation*, 53(4):303–308, 2000.

[26] M. Herty. Modeling, simulation and optimization of gas networks with compressors. *Networks and Heterogeneous Media*, 2(1):81, 2007.

[27] J. Zhou and M. Adewumi. Simulation of transients in natural gas pipelines using hybrid tvd schemes. *International journal for numerical methods in fluids*, 32(4):407–437, 2000.

[28] A. R. Thorley and C. H. Tiley. Unsteady and transient flow of compressible fluids in pipelinesa review of theoretical and some experimental studies. *International journal of heat and fluid flow*, 8(1):3–15, 1987.

[29] H. Rachford and R. Carter. Optimizing pipeline control in transient gas flow. *Pipeline Simulation Interest Group*, 2000.

[30] M. Abbaspour, P. Krishnaswami, and K.S. Chapman. Transient optimization in natural gas compressor stations for linepack operation. *Journal of Energy Resources Technology*, 129(4):314, 2007.

[31] P. Domschke, O. Kolb, and J. Lang. Adjoint-based error control for the simulation and optimization of gas and water supply networks. *Applied Mathematics and Computation*, 259:1003–1018, 2015.

[32] K. Ehrhardt and M. Steinbach. *Nonlinear optimization in gas networks*. Springer, 2005.

[33] M. Steinbach. On pde solution in transient optimization of gas networks. *Journal of computational and applied mathematics*, 203(2):345–361, 2007.

[34] A. Zlotnik, M. Chertkov, and S. Backhaus. Optimal control of transient flow in natural gas networks. In *54th IEEE Conference on Decision and Control*, pages 4563–4570, Osaka, Japan, 2015.

[35] T. W. K. Mak, P. Van Hentenryck, A. Zlotnik, H. Hijazi, and R. Bent. Efficient dynamic compressor optimization in natural gas transmission systems. In *IEEE American Control Conference*, pages 7484–7491, Boston, MA, 2016.

[36] S. Grundel, N. Hornung, B. Klaassen, P. Benner, and T. Clees. Computing surrogates for gas network simulation using model order reduction. In *Surrogate-Based Modeling and Optimization*, pages 189–212. Springer, 2013.

[37] Q. Gong, F. Fahroo, and I. M. Ross. Spectral algorithm for pseudospectral methods in optimal control. *Journal of Guidance, Control, and Dynamics*, 31(3):460–471, 2008.

[38] C. Canuto, M. Y. Hussaini, A. Quarteroni, and T. Zang. Spectral methods. *Fundamentals in Single Domains, Springer*, 2006.

[39] Q. Gong, W. Kang, N. S. Bedrossian, F. Fahroo, P. Sekhavat, and K. Bollino. Pseudospectral optimal control for military and industrial applications. In *Decision and Control, 2007 46th IEEE Conference on*, pages 4128–4142. IEEE, 2007.

[40] J. G. Verwer and J. M. Sanz-Serna. Convergence of method of lines approximations to partial differential equations. *Computing*, 33(3-4):297–313, 1984.

[41] A. Wächter and L. T. Biegler. On the implementation of an interior-point filter line-search algorithm for large-scale nonlinear programming. *Mathematical Programming*, 106(1):25–57, 2006.

[42] S. Grundel, L. Jansen, N. Hornung, T. Clees, C. Tischendorf, and P. Benner. Model order reduction of differential algebraic equations arising from the simulation of gas transport networks. In *Progress in Differential-Algebraic Equations*, pages 183–205. Springer, 2014.

[43] A. Zlotnik, S. Dyachenko, S. Backhaus, and M. Chertkov. Model reduction and optimization of natural gas pipeline dynamics. In *ASME Dynamic Systems and Control Conference*, page V003T39A002, Columbus, OH, 2015.

[44] M. Abbaspour and K.S. Chapman. Nonisothermal transient flow in natural gas pipeline. *Journal of Applied Mechanics, Transactions of the ASME*, 75(3), May 2008.

[45] E. S. Menon. *Gas pipeline hydraulics*. CRC Press, 2005.

[46] A. Zlotnik, A. M. Rudkevich, E. Goldis, P. A. Ruiz, M. Caramanis, R. Carter, S. Backhaus, R. Tabors, R. Hornby, and D. Baldwin. Economic optimization of intra-day gas pipeline flow schedules using transient flow models. In *Proceedings of PSIG Meeting, Atlanta, GA*, 2017.

[47] G. Elnagar, M. Kazemi, and M. Razzaghi. The pseudospectral legendre method for discretizing optimal control problems. *Automatic Control, IEEE Transactions on*, 40(10):1793–1796, 1995.

[48] B. Fornberg. *A practical guide to pseudospectral methods*, volume 1. Cambridge university press, 1998.

[49] Q. Gong, F. Fahroo, and I. M. Ross. Spectral algorithm for pseudospectral methods in optimal control. *Journal of Guidance, Control, and Dynamics*, 31(3):460–471, 2008.

[50] R. Fourer, D. M. Gay, and B. W. Kernighan. *AMPL: A Modeling Language for Mathematical Programming*. Cengage Learning, 2002.

[51] AMPL. AMPL Optimization: `http://www.ampl.com`, 2014.

[52] M. Pfetsch, A. Fügenschuh, B. Geißler, N. Geißler, R. Gollmer, B. Hiller, J. Humpola, T. Koch, T. Lehmann, A. Martin, A. Morsi, J. Rövekamp, L. Schewe, M Schmidt, R. Schultz, R. Schwarz, J. Schweiger, C. Stangl, M. Steinbach, S. Vigerske, and B. Willert. Validation of nominations in gas network optimization: Models, methods, and solutions. *Optimization Methods and Software*, 30(1):15–53, 2015.

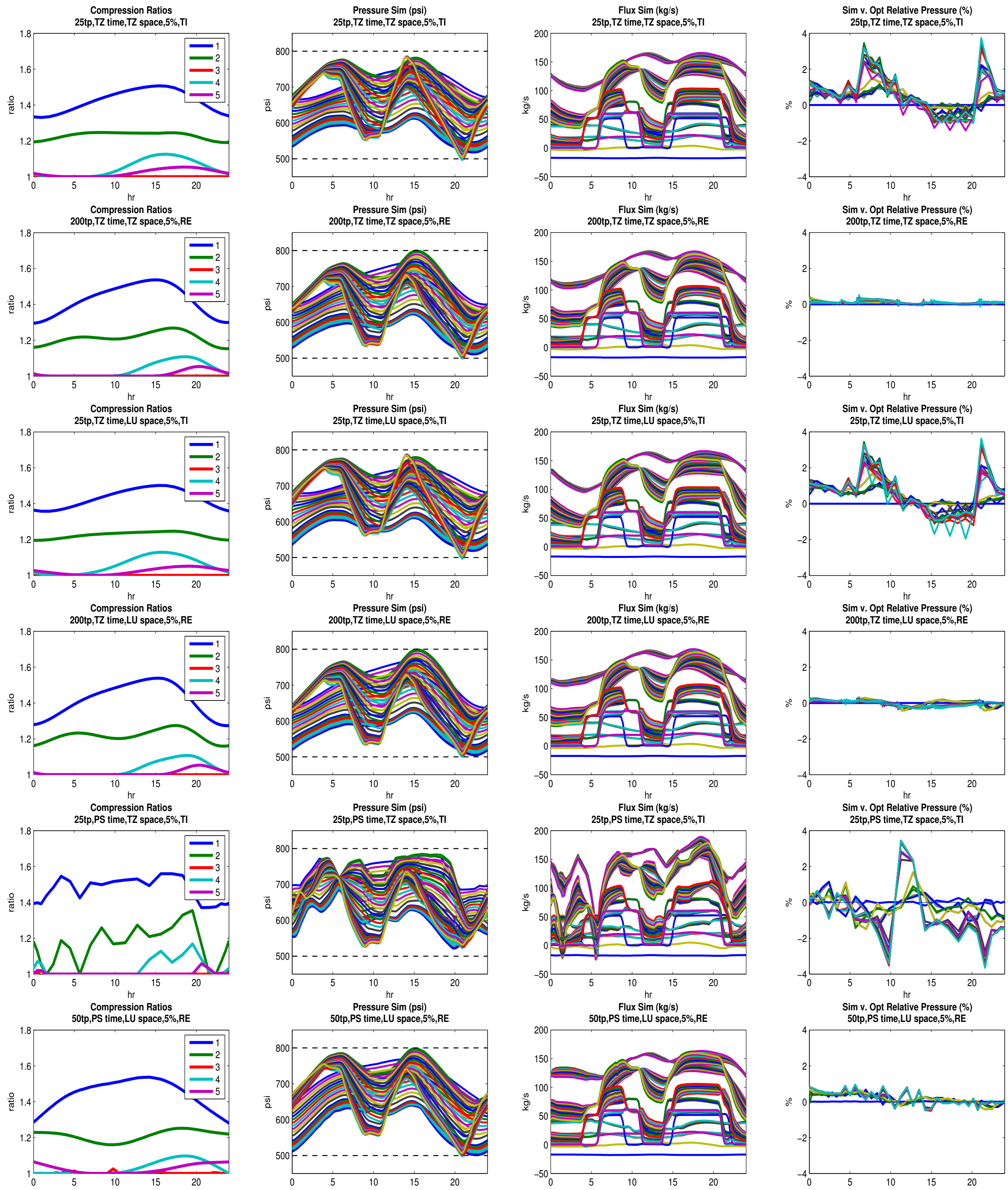

Figure 3 **From top to bottom (24-System): Various discretization schemes: trapezoidal rule with various numbers of time points (tp), trapezoidal(TZ)/pseudospectral(PS) time scheme, trapezoidal(TZ)/lumped element(LU) space scheme, 5% re-optimization tolerance, and tightened(TI)/regular(RE) constraints. From left to right: Optimal compressor ratios; Pressure trajectories from simulation using the controls; Flux trajectories from the same simulation; Relative difference between pressure solution from optimization and pressure trajectories from simulation.**

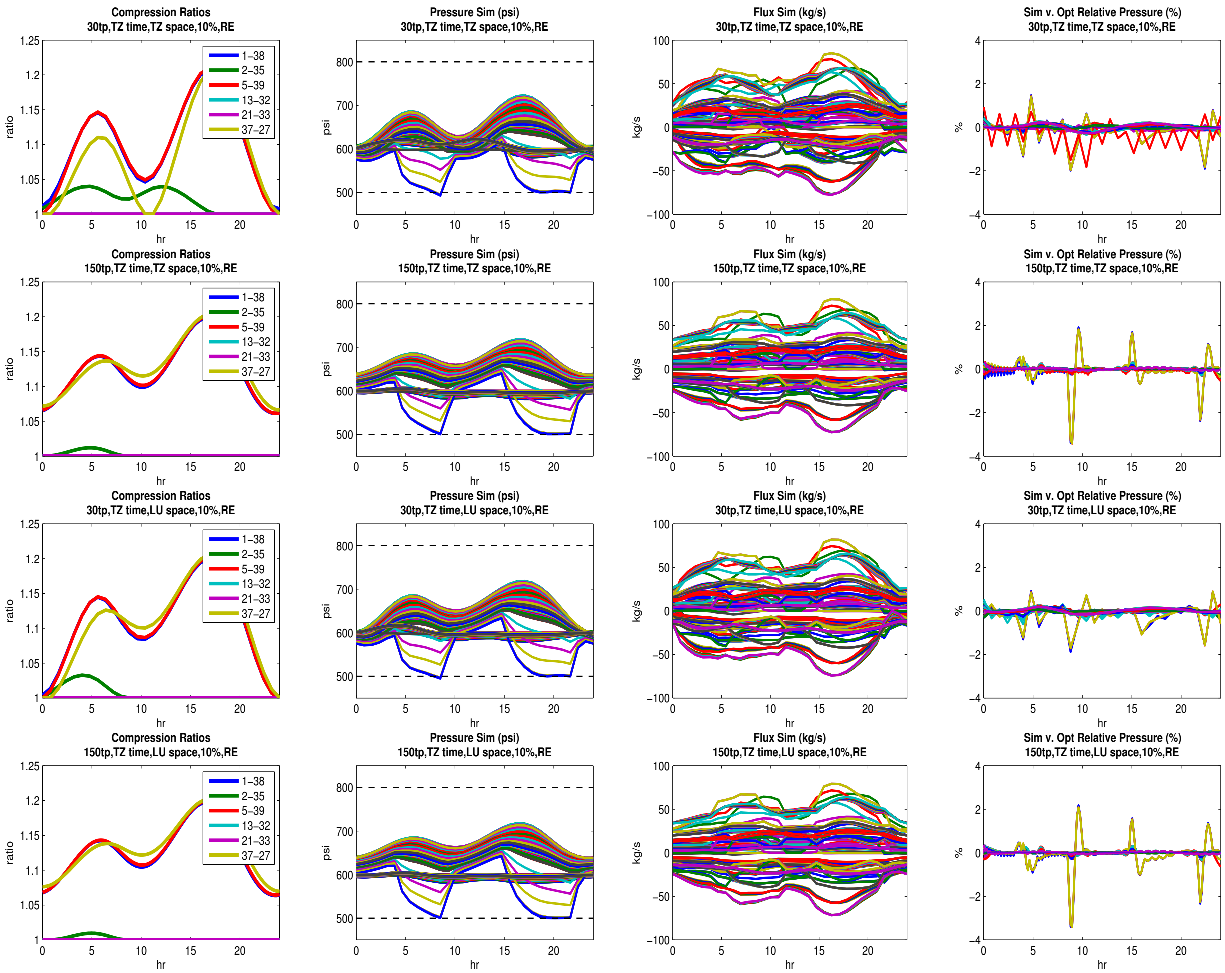

Figure 4 From top to bottom (Gaslib-40):: Various discretization schemes with: 30 and 150 time points (tp), trapezoidal(TZ) time scheme, trapezoidal(TZ) and lumped element(LU) space scheme, and 10% re-optimization tolerance. From left to right: Optimal control solution; Pressure trajectories from simulation using the controls; Flux trajectories from the same simulation; Relative difference between pressure solution from optimization and pressure trajectories from simulation.

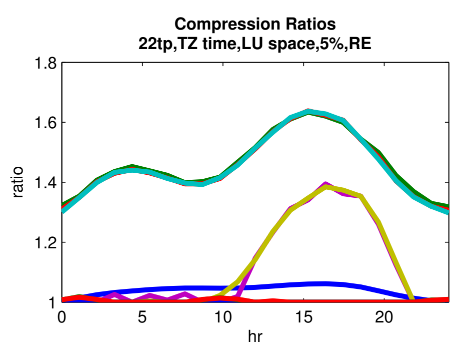

Figure 5 Compression ratio solutions for Gaslib-135 case studies, with 22 trapezoidal (TZ) time points, lumped element (LU) space, and re-optimization tolerance of $r = 5\%$.

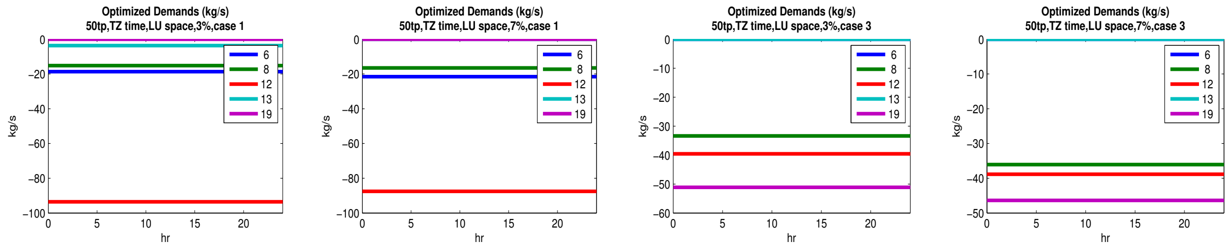

Figure 6 Optimized demands(kg/s). From left to right: case 1: $r = 3\%$ and 7%, and case 3: $r = 3\%$ and 7%.

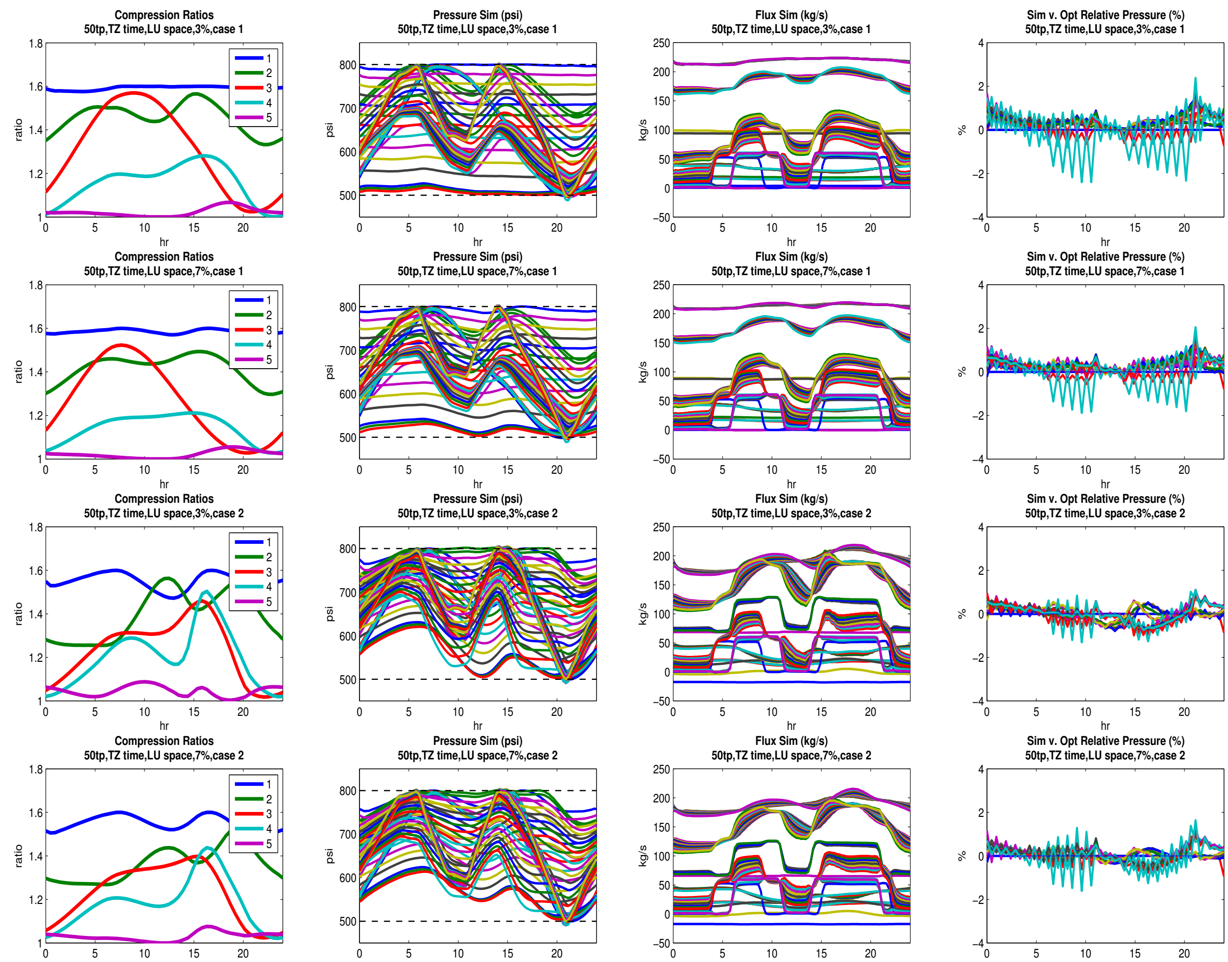

Figure 7 From top to bottom: Case 1 with 3% and 7% re-optimization tolerance, and case 2 with 3% and 7% re-optimization tolerance. Both with 50 trapezoidal time point, and lumped space approximation.

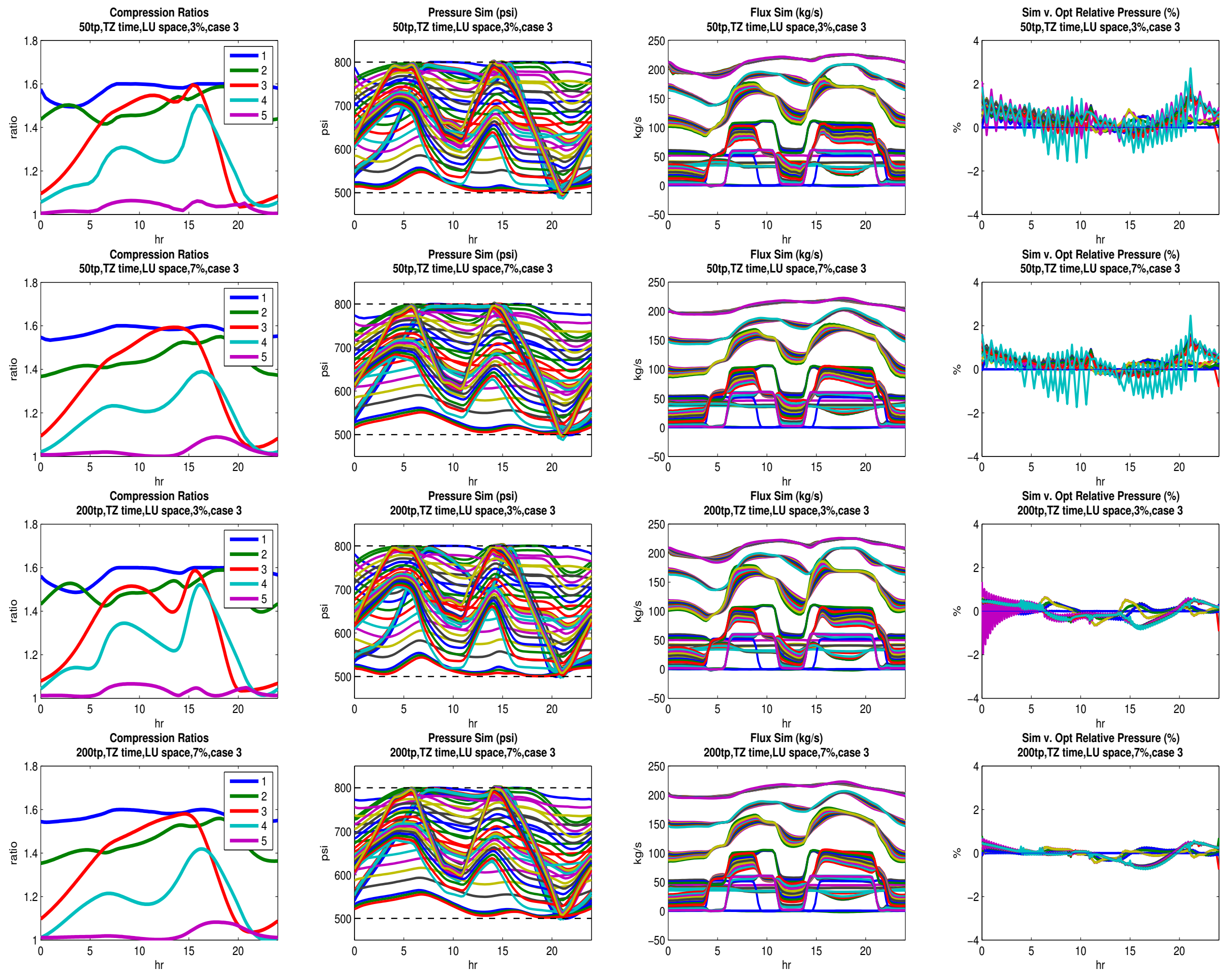

Figure 8 From top to bottom: Case 3 with 3% and 7% re-optimization, 50 trapezoidal time point, and lumped space approximation; Case 3 with 3% and 7% re-optimization, 200 trapezoidal time point, and lumped space approximation.